ANIMATED-TEM: a toolbox for electron microscope automation based on image analysis

Gilles Hermann, Nicolas Coudray, Jean-Luc Buessler, Daniel Caujolle-Bert, Hervé W. Rémigy, Jean-Philippe Urban

ANIMATED-TEM: a toolbox for electron microscope automation based on image analysis

Gilles Hermann[a], Nicolas Coudray[a], Jean-Luc Buessler[a], Daniel Caujolle-Bert[b], Hervé-W. Rémigy[b,c], Jean-Philippe Urban[a]

[a] MIPS laboratory, University of Haute Alsace, Mulhouse, France

[b] C-CINA - M.E. Mueller Institute for Structural Biology, Biozentrum, University of Basel, Switzerland

[c] FEI Electron Optics BV, Eindhoven, Netherlands

Abstract – This article presents the ANIMATED-TEM (ANalysis of IMages for Automatic Targeting and Extraction of Data in Transmission Electron Microscopy). This software package is composed of a set of image analysis algorithms for target selection and characterization of biological sample in transmission electron microscopy. Combined with a microscope control software package, it selects automatically regions of interest at appropriate magnification. Acting as a supervisor, ANIMATED-TEM controls the microscope tasks (stage displacement, magnification, etc.), localizes the regions of interest and manages the sample exploration strategy. Data are extracted at different magnifications to assess the grid quality at low magnification, the characteristics of the biological samples at medium magnification (membrane size, shape, and stacking-level), and the crystallinity at high magnification (identification of diffraction peaks). Grid quality and sample features are used to trigger new acquisitions at higher magnifications. These tools have been developed to allow high-throughput screening of 2D-crystallization experiments; the microscope is equipped with a grid-autoloader, allowing the automatic analysis of 96 samples. The toolbox is operational; the testing conducted for several months confirms that the image analysis achieves a full automation with an efficient target selection and a limited computational time for image analysis.

Keywords – Automated image acquisition; Transmission Electron Microscope; Target selection; Specimen characterization; Fully automated electron microscope

1. Introduction

This article presents a software toolbox for the automation of an electron microscope. All the examination steps of a biological sample are entirely

autonomous. An autoloader system attached to the microscope allows the continuous processing of a set of 96 grids without human intervention.

Each examination step corresponds to the acquisition and analysis of one image. All data, the measured characteristics as well as the images, are stored and managed by a database system that allows the biologist to verify the analysis a posteriori, and if required, to reload and resume the sample observation. A typical 96-grids run acquires about 6000 images, taking 54 hours, corresponding to a mean time of 34 minutes per sample. The run time and the number of image acquisitions are strongly tied to the quality of the sample and the protocol parameters, as will be specified further in the text.

ANIMATED-TEM (ANalysis of IMages for Automatic Targeting and Extraction of Data in Transmission Electron Microscopy) triggers micrographs acquisition and analyses them to evaluate the sample quality, but is also able to fully control the microscope. The main innovation of the ANIMATED-TEM toolbox is the automated online image analysis including the decision steps for grid examination. The automation technique mimics the strategy of a microscopist that selects potentially interesting regions at various magnifications. The objects being generally scarce and scattered randomly on the grid, it is not realistic to pre-define regions randomly nor to examine a grid systematically. The objects must be localized by analyzing the images acquired with the integrated CCD camera.

The design of algorithms for electron microscopy image analysis is a current challenging issue, both for its difficulty and the great potential is shows. Manufacturers offer microscopes interfaced to CCD cameras that are entirely software controlled, with performances suitable for automation. Several recent publications introduce very interesting tools for the automated acquisition of images (e.g., [1-3]). For an entirely autonomous control that is intelligent enough to adapt to each sample, image interpretation must be introduced, at least partial image interpretation. Therefore computer vision for electron microscopy needs to be devised.

Image processing in electron microscopy appeared to be really challenging and led us to develop several original algorithms to solve the problem of localizing objects that are hard to detect, even for the expert eye. The difficulties are caused by the high level of noise in the images, the weak contrast of the biological objects, and the absence of texture or precise characteristics that would identify

the objects searched for. As it appears commonly in computer vision tasks, the organization of the image data analysis steps is highly application dependent. The processing chain that we present is dedicated to detecting artificial membranes and testing if these membranes present a periodical structure.

Our algorithms would need to be adapted to visualize other objects in an electron microscopy context. The purpose of the ANIMATED-TEM toolbox is to provide an efficient tool for the study of bi-dimensional crystallization conditions of membrane proteins, part of a European Union project (HT3DEM), and more generally for the testing and validation of an actual TEM automation implementation.

The HT3DEM (High-throughput three-dimensional Electron Microscopy) project resulted in the implementation of a robotic platform for the bi-dimensional crystallization of membrane proteins. This approach uses crystallographic techniques to study the three-dimensional structure of proteins that are reconstituted in the presence of lipids to form artificial membranes. The determination of bi-dimensional crystallization conditions requires a large number of trials that compels automation.

The HT3DEM toolchain includes: i. the DropBox, a device to assess accurately the amount of detergent needed to purify a membrane protein, ii. The Ternary Mixture Robot, a machine mixing automatically the purified protein with various lipids and additives, as membrane proteins are reconstituted in the presence of lipids to form artificial membranes, iii. the 2DX Robot, a crystallization robot based on the neutralization of the detergent by Cyclodextrin, iv. the Staining Robot, a machine preparing the crystalline samples made by the 2DX Robot on special grids suitable for EM screening.

ANIMATED-TEM contributes to the final link of this robotization chain and automates the examination step of each sample with the electron microscope to evaluate crystallization.

The scientific effort towards full TEM automation is overviewed in section 2. The main image processing tools to achieve automation are briefly introduced in section 3, followed in section 4 by the description of the architecture of the fully automated microscope control. Section 5 presents the results and experiments

conducted on the experimental platform, illustrating the performances achieved by ANIMATED-TEM toolbox.

2. Towards full TEM automation – State of the art

Several recent works illustrate the effort of the scientific community to automate tasks in electron microscopy. The application fields remain somewhat limited, and concentrate on a number of specific fields. Among them, the study of the three-dimensional structure of proteins is the most illustrative example. Indeed, different techniques – tomography, single particles, and crystallization – are the subject of specific and long term efforts for the development of software tools. The evolution of certain software toolboxes over the years shows both the magnitude of the task at hand and the increasing importance played by computer vision.

Today's electron microscopes are microprocessor controlled and can therefore be controlled by external software. The generalization of digital cameras opens the possibility to automate the acquisitions. A complementary step towards autonomy is the recent appearance of loading systems to insert specimens into the microscope. Potter et al.[4] use a robotic arm that reproduces the human grid insertion gesture. Lefman et al. [5] describe a motorized cartridge holder of 100 samples for rapid specimen exchange. In this project, we use a Tecnai T12 equiped with an carousel which can host up to 8 cassettes, for a total of 96 grids [6].

The first software tools for the control of a TEM have been devised for the automation of repetitive data acquisition tasks by executing scripts [7-9] and to create dedicated interfaces for specific techniques like tomography [10, 11]. Image processing has first been used to design auto-tuning methods for accurately setting astigmatism, focus, and alignment of the TEM. Koster [7] introduced a correction of image shifts resulting from tilting the specimen in tomographic series data.

With the evolution of image processing techniques and strong increase and availability of computational power, the interpretation of images becomes of growing importance. It allows to improve auto-tuning techniques (e.g., Mastronarde [12], for correction techniques in tomography) but mostly to address

new purposes. Image classification, interpretation or software evaluation become literally a necessity to process the thousands of images recorded by certain semi-automated systems, like the one proposed by Oostergetel et al. [13]. Anderson et al. [14] describe an ambitious project of automated analysis of the neural circuitry reconstruction by assembling thousands of TEM images. The single particle technique [15] is strongly based on computer vision techniques to reconstruct the three-dimensional structure of macromolecules. The principle is to average a large number of identical particles to compensate for the insufficient precision of the electron microscope. However, as the reconstructed resolution approaches the atomic level, hundreds of thousands of particles may be necessary. The manual selection of particles in micrographs becomes too tedious. Detection algorithms have been the subject of much research work compiled in [16].

To automate the microscopy tasks entirely, the software must make the decisions in place of the human expert. The interpretation of the image must therefore be done in real time to make choices during the examination of the sample. Although these decisions are often limited, very repetitive and application-dependent, it is still challenging to replace the expert with computational approaches. Two fields, electron tomography and single particles, illustrate well the state of the art, and they are both the subject of important developments.

In the field of electron tomography, the automation and integration of software tools in a unified interface is well advanced [3, 17], and manufacturers, like FEI, offer software packages for tomogram acquisition and reconstruction. The sequential tilt-series acquisition is fully automated. Recent software packages enable to chain several series, advancing from one target to another. Three-dimensional reconstructions are produced in real time and user intervention to set markers for reconstruction could be suppressed recently [18]. The automation is therefore almost total, the selection of targets remaining the responsibility of the user. Even though this work is eased by an optimal organization gathering the selections at the beginning of the session and an efficient software assistance [17], it seems not yet possible to replace it by a reliable algorithm.

The technique of single particles almost benefits from a full automation when the macromolecules to be detected are localized on a carbon film, with regular holes. The selection procedure determines successively the good squares, then the holes containing suitable and uniform ice layers. Some toolboxes, although offering

efficient software assistance, remain semi-automated (e.g. [5, 19]). They require a selection phase where the user picks interesting holes from images. Other toolboxes [1, 2, 20] recently introduced an entirely automated mode using a computational image analysis for the selection task. But their designers remain cautious and do not consider their technique reliable enough. Thus, AutoEM [20] is configured by default in semi-automated mode; JADAS [2] proposes an automated selection after manually setting the image intensity criterion and calibrating parameters as diameter of a hole, the distance between neighboring holes, etc. Even with the success of the automation, Zhang, et al., write that "the presence of trained user or the availability of an intelligent real-time data assessment software is still necessary to assure the data quality". Stagg, et al. [21], on the other hand, report the satisfactory performance of this selection with the Leginon software package [1].

The important noise and the intensity fluctuations represent the main difficulties to extract reliable information from CCD micrographs. The localization of the holes is simplified by the regular geometry of the grid and a fixed hole diameter and their periodical organization. However, the selection of suitable holes is delicate. The cited software packages all use the mean value and the variance of the image intensity within the hole.

In many other applications of electron microscopy, the objects of interest are more complex and not localized by a regular structure. The challenge for computer vision is therefore all the more important. The automation of the analysis of bi-dimensional crystal samples is one example [22, 23]. The work presented in our article is the first to integrate a fully automated selection of targets.

We close this section with the analysis technique introduced by Kylberg [24] for the first two levels of magnification of an automated virus diagnosis system. The overview images of the grid are first analyzed to precisely localize and select good squares. At higher magnification, an empirical analysis of the problem leads to the formulation of a few simple rules: regions with a higher probability to contain small clusters of viruses are identified by detecting objects that are somewhat circular and of diameter in a given range. The algorithms have not yet been integrated in a control system, but seem promising.

3. Presentation of the image processing tools

The main image processing tools to achieve a full automation of a TEM are briefly introduced in this section. These algorithms are able to adapt to the various types of membranes and to the possible fluctuations of the acquisition parameters, based on a few known characteristics of the samples. All parameters are pre-determined or automatically adjusted, e.g. thresholds, such as the system runs without human intervention at any time.

Automatic analysis of a specimen requires the acquisition of images at different magnifications and their direct processing to determine successively the regions of interest. In this section we present an overview of the tools we developed for the three levels of magnification [25].

3.1 Low magnification image analysis

At low magnification (field of view of at least 300x300µm for 1024x1024 pixel images), images of mesh grids typically used in TEM experiments are analyzed to assess the quality of the overall grid and retain a number of regions for further analysis. In particular, regions where the carbon film is locally broken must be discarded (see Figure 1).

A three-step algorithm uses the gray-level histogram to automatically select the various thresholds. First, the grid squares are segmented using a global threshold positioned after the first peak of the histogram (representing the copper bars). Second, the background of each grid square, i.e. the brightest region represented by the last peak of the local histogram, is segmented using a local threshold. Each square is classified in three classes: broken carbon film, valid membranes, and unknown. From the first two classes, typical gray-levels of backgrounds are extracted. Third, these gray-level statistics are used to classify squares previously labeled as unknown.

This analysis outputs the proportion of good grid squares for the characterization, and their coordinates for medium-magnification targeting.

3.2 Medium magnification image analysis

At medium magnification (field of view ≈ 15x15µm), images of membranes are processed through a chain of algorithms: a segmentation step made of a newly developed contour detection algorithm supplemented by a false edge removal

phase [2-28], followed by two labeling steps to identify the foreground region and to characterize its stacking [29]. Once membrane regions are isolated, other characteristics such as size and shape can be extracted. For the automatic targeting, regions of interest (ROI) selected are the coordinates of the largest non-stacked membrane regions.

A thorough and complex image analysis is not always necessary to select the ROI. In [25] we describe a fast procedure to select potentially crystalline regions by simply avoiding background regions (no information) and dark regions (artifacts, important aggregates or stacking, etc.) and selecting ROI inside the objects near background edges. The Partial Edge Detection (PED) process selects ROI near edges detected by a Prewitt filter, as long as the region is not too dark (i.e. above a threshold experimentally set).

In this section, we describe a more precise method to select potentially crystalline regions (cf. [25] for a detailed description).

These target regions being identified by distinct properties (in term of size, shape, etc.), the procedure requires a precise segmentation and characterization of the biological objects present in the image. The chain of algorithms used is presented in Figure 2. The principle of the algorithms is given in the next paragraphs.

Contour detection

Because of the nature of the TEM images (very noisy, low-contrasted, heterogeneous gray-levels), a new algorithm based on a multi-scale approach has been devised especially to detect the contours in these difficult images [27].

To identify all types of contrasted edges, gradient images, obtained at different scales of a pyramidal transform, are thresholded using the T-point algorithm [26]. This algorithm outputs the threshold of unimodal histogram images in a robust manner, practically insensitive to noise distribution, histogram fluctuations and quantity of edges to segment. The different resulting binary images are combined in one image, called reconstructed gradient-like (RGL), where the gray-level is proportional to the scale at which the edge has been identified. A finer scale corresponds to a higher gray-level, which leads to a more precise positioning of the contour. The final splitting and contour positioning is achieved by applying the watershed algorithm to the RGL image. On the resulting image (Figure 3B), this method allows the identification of most of the regions, even the lowest

contrasted ones. The downside of the approach is that, even though they are few, generating false edges cannot be avoided.

False Edge removal

The second algorithm will remove the spurious edges introduced by the contour detection method using a statistical analysis of the local contrasts [28]. Each segment of the partitioned image, i.e. each set of contour pixels separating two regions, is analyzed: if the segment is relevant, a regular and coherent gradient perpendicular to this segment can be observed; in the case of a false segment, the gradient is either absent, or it exists only partially, or it is incoherent along the segment. The contour segments are validated using in the following algorithm: i) a mask is created from the orientation evaluation of the contour pixels and the one-dimensional profile of the reference potential contour is extracted according to this mask. ii) a correlation measure between the profile and a reference filter is achieved. iii) the correlation factor, averaged over all segment pixels, is compared to a threshold derived from statistical hypothesis testing to take image noise into account. Segments whose correlation factor is below this threshold are removed (Figure 3C).

Stacking level determination

Once the image is properly partitioned, the specimen can be characterized. In the third step of the chain, regions are labeled: after having identified the background, foreground regions are classified according to the number of superposed objects by the stacking level. The background is temporarily identified as the brightest and largest region [30]. The labeling of the remaining regions is achieved using an iterative algorithm [29]. This algorithm achieves a labeling of the regions according to their stacking level, and it also completes the background detection by detecting smaller background regions. Each iteration of the algorithm is made of two steps, and corresponds to the identification of regions belonging to a given stacking level. To accomplish the classification of the regions, thresholds have to be set. In the first step, using a priori knowledge, we select a set of regions whose probability of belonging to the searched stacking level is high. These regions are used to identify the typical contrast of such regions. In the second step, this typical contrast is used to compute the threshold and refine the classification. This result

is the labeling of each region according to its relative stacking level within the image (Figure 3D).

Linear and circular shapes

In the last step of the characterization, an algorithm has been developed to locally assess the shapes of the contours of the biological objects [31]. Since biological objects are randomly deposited on the support, they are often adjacent, partially superposed, or stacked. Therefore, the shapes can only be evaluated by analyzing locally the objects in contact with the background. Contours inside the foreground cannot be used to separate adjacent objects, as a contour line may represent a fold inside a folded object and not the object's outline. Shapes of the external contours are divided, when possible, into coherent "linear" or "circular" sections. A recursive method based on shape regression is used to identify if the contours can be approximated locally by lines or arc of circles (Figure 3E).

These characteristics are used to determine the regions that correspond, with the best probability, to well spread out membranes, not superposed, and crystalline, therefore interesting regions to validate the crystallization conditions of the sample. An empirical sorting rule has been devised for region classification (see section 5.2). The primary regions are retained for the next analysis step at high magnification.

3.3 High magnification image analysis

This is the final step where images are acquired at high magnification (around x30.000, i.e. 0.5 nm/pixels) in order to assess the sample quality. Crystallinity can be automatically checked with a process analyzing the Fourier Transform (FT) of images acquired at high magnification. However, TEM Contrast Transfer Function (CTF) prevents simple thresholding of the FT. CTF generates a heterogeneous background, called the Thon rings, which should be removed first. CTF is assessed by computing the average radial profile of the FT. This profile is then used to reconstruct the 2D CTF and subtract it from the original FT. The obtained corrected FT is finally thresholded to identify diffraction peaks. By default, the threshold is set to identify peaks whose signal-to-noise ratio is above 3.5 (false detections become important below this threshold because of the noise). The user can optionally adjust this value.

4. Fully automated microscope control

The tools presented in section 3 have been assembled and organized to form the ANIMATED-TEM software presented here. It has been developed as a Matlab Toolbox (R2008a), requiring the Image Processing Toolbox. It has been developed to analyze the images acquired and achieves two goals:

(1) Automatic targeting: identify the ROI to be acquired at higher magnification to assess the crystallization experiment. Coordinates of the targeted regions are transmitted to the control system for further acquisition.

(2) Automatic Extraction of Data for sample characterization: images selected and analyzed at different magnifications are used to assess the support (grid's carbon film), the detected membranes, and check their crystallinity through the diffraction pattern.

ANIMATED-TEM has been integrated on a prototype located at the C-CINA, Basel. The on-line automatic control consists of the interaction between three systems: the TEM and two computers, one for the microscope control tools, and one for the analysis of the images achieved by ANIMATED-TEM. The software interacts with the microscope control tools by sending HTTP requests corresponding to the desired action (stage displacement, image acquisition magnification to be set, etc.) The microscope control computer controls physically the devices of the TEM according to the requests received. It also transmits to the image processing computer the images acquired by the CCD camera.

The Tecnai T12 microscope is equipped with a 1kx1k CCD, and with unique autoloader and carousel. The carousel encloses 8 cassettes of 12 grids. Cassettes can be inserted consecutively into the autoloader which then controls the loading of the grid into the microscope, enabling to control the microscope for a fully autonomous acquisition of images from 96 different samples. The microscope control tools achieve the physical command of the microscope (stage displacement, image acquisition, magnification setting…). ANIMATED-TEM processes the images acquired, and decides when, where, and how images should be acquired.

In the first subsection below, the microscope control tools are briefly presented. The second subsection develops the scenario monitoring the automatic acquisition and introduces the GUIs (Graphical User Interfaces).

4.1 Microscope control

Presentation

The microscope control tools have been developed to interface our image processing tools and the microscope as presented in Figure 4. The software, called JusT12, interacting with the microscope is using the FEI automation servers. An additional server has been developed to control the 12-cassette carousel. COM technology permits to access remotely other computers, but it introduces network latency. Hence, the JusT12 software installed on the microscope computer has been written, and designed to react to HTTP requests. Also, the choice has been made to separate the microscope control code from ANIMATED-TEM to keep the matlab code as clean as possible, and to delegate the microscope control to a dedicated software which made it easier to maintain.

"Semantic" commands are those received from ANIMATED-TEM via an HTTP interface. They include the name of the physical command to be performed, and the required parameters (for instance the coordinates of the new position, the index of the grid to be loaded, the amount of illumination, the value of the stage displacement, the magnification, etc.). We note that during the stage displacement, a backlash correction is achieved by always moving to the desired target from the same direction.

Therefore, the Image Processing part sends HTTP requests to the Microscope Control part that manages TEM devices. If an image acquisition has been requested, the 1k x 1k image acquired with a CCD camera is transferred to the Image Processing computer for analysis and storage.

Carousel Graphical User Interface

A carousel control GUI has been developed to:

• initialize the position of the 8 cassettes within the carousel (Figure 6, right): initialization is one of the first steps to do once the carousel is installed on the

microscope. The initial positioning adjustment is robust and still valid in our T12 prototype since its initial installation and initialization.

• visualize the state of the machine and the sensors;

• manually control the carousel and the cassette (un)loading: this feature can be used if the user does not use the automatic process, or to take control of the carousel if there is a problem during the automatic process. More than a thousand loadings and unloadings have been automatically and manually performed so far without any problem.

4.2 Automatic run scenario

Presentation

The scenario aims to articulate the different algorithms and allow an on-line image computation of up to 96 grids in a fully automated manner. The scenario has been elaborated to generate the semantic command (acquire image, move microscope, etc.) at the appropriate moment.

The scenario can be decomposed into 4 parts: grid loading (part 1) and specific processing (part 2-4) for each magnification. Figure 6 shows typical acquisitions for this scenario. The flowchart in Figure 7 details each step.

This flowchart has a certain number of loops; the amount of iterations depends on the result of the image processing, and on parameters set by the user before launching the automatic run (as presented in the next section).

As shown in the flowchart, the low-, medium-, and high-magnification steps are made of three parts:

• the managing of the iterations (amount of images acquired).

• the semantic commands to move the stages to the desired targets, and to acquire the images (this latter includes the commands of the exposure time, illumination, defocus): at high and medium magnification, positions are determined by the image processing achieved at the previous magnification. At low magnification, images are acquired according to a circular-like pattern, as shown in Figure 8.

• the processing of the images, using the tools presented in the previous section.

Main Graphical User Interfaces

Two graphical user interface (GUI) are used: one to launch the automatic run and set some parameters, the other to visualize the results.

GUI - Launcher

Through the GUI Launcher, the user can pre-set parameters to meet the requirements of the above described basic scenario. Among the default parameters that can be changed, we note:

• the stop criteria which define how many grid squares should be visited at medium magnification (limit for ∑MM), or the maximum number of low-magnification images to acquire (limit for LM);

• the maximum number r of ROI to identify at medium magnification and the algorithm to use (the PED and/or the multi-resolution-based method);

• the grids g which should be analyzed during the run;

• the acquisition parameters (illumination, exposure time, etc.).

As will be seen in the experimental result section, these parameters greatly influence the time spent by the automatic run.

Setting up the ANIMATED-TEM toolbox for other microscopes may require only a few adaptations of the parameters (depending on the autoloader of the microscope), and of the instructions used to send the semantic commands (depending on the microscope control tools).

GUI - Browser

A GUI Browser has been developed to view the images automatically acquired. The interface links images to the corresponding acquisition at lower or higher magnification. The user can reload a selected grid and move it to the position where the current image has been acquired.

A pop-up window can be opened to display statistical characteristics concerning the run and the sample. For each grid it gives the time spent for its screening; the number of images acquired; the estimations of the percentage of good-quality grid squares; and the average size of non-stacked membrane regions.

5. Results and experiments

ANIMATED-TEM toolbox is used to control a customized Tecnai 12 microscope equipped with an autoloader and a carousel, which allow to treat automatically up to 96 grids. During the testing phase, over 66,000 images have been treated, corresponding to approximately 1,500 grids analyzed in 230 runs.

This section focuses principally on 2 features: the time required for each step during a run, and the automatic determination of the regions used for next examination, the ROI, which is an essential point of our original automation approach.

5.1 Run time

The overall time spent on an automatic run mainly depends on two parameters: the settings defined by the user (maximum amount of images and regions of interest), and the results of the image processing (actual amount of targets identified, related to the quality of the grid and to the interest of the sample at medium magnification).

Successive acquisitions at low-, medium-, and high-magnification will be processed according to the control strategy defined initially using the GUI.

The processing time can be approximated as follows:

$$T = \left(N_{LM} \cdot T_{LM} + N_{MM} \cdot T_{MM} + N_{HM} \cdot T_{HM} + N_F \cdot T_F \right) \cdot N_G + N_C \cdot T_C + N_G \cdot T_G \ ,$$

with:

- N_{LM} , N_{MM} , and N_{HM} , respectively the amount of images acquired at low, medium, and high magnification;
- T_{LM} , T_{MM} , and T_{HM} , the average times for acquisition and processing;
- N_F , and T_F , the number of executions and the execution time of the autofocus process at high magnification;
- N_G , and T_G , the amount of grids an the loading time of a grid;
- N_C , and T_C , the amount of cassettes and the loading time of a cassette.

Figure 11 gives a chronogram of a grid analysis leading to the acquisition of 10 images. In white, we show the microscope control times, and in black the image processing times. The average times required at low, medium and high magnification are respectively 20s, 27s, and 40s.

The times displayed here are obtained on an Intel Xeon processor at 2.67 GHz & 6 Gbytes of RAM computer, on large images (1k x 1k images). Processing larger images may require adaptations to cope with the important memory required.
In the example of Figure 11, image 1 allows the selection of two targets (images 2 and 5) that will trigger the next acquisitions at medium magnification. On the contrary, image 7 (low magnification) does not allow a correct target selection, so a new image has to be acquired at low magnification (image 8).

Average times for microscope control and image acquisition

It takes about $T_G \approx 180$s to insert a grid into the microscope, and about $T_C \approx 300$s to insert a cassette into the autoloader.
Table 1 shows the times for the execution of the physical commands on the first row. Average times for microscope control and image acquisition include the setting of the acquisition parameters (magnification, exposure time, illumination, and defocus), the stage displacement, and the image acquisition. The last two steps are the most time-consuming. Only the time spent for image acquisition could be reduced by using a faster camera (we estimate a gain of about 5 seconds). The greater distances to travel at low magnification can explain the difference between average times at low and medium magnification. At high magnification, the average time also includes the autofocusing step which are time-consuming (up to T_F =50s). An improved method for autofocusing would reduce this delay. We notice that its influence on the overall time can be reduced by modifying the frequency of the autofocusing measurement. When high-magnification images are acquired consecutively, their positions are close enough to avoid focusing before each acquisition. An option in the GUI Launcher presented previously can be used to decide if the measurement should be done before each high-magnification acquisition or not.

Average time for image processing

The strategy used for the grid analysis is to acquire a low-magnification image in order to assess the quality of the grid and to establish the list of valid grid squares to be examined at higher magnification. At low magnification, more than 99 % of the selected grid squares are non-broken carbon film regions. Such a high result

implies two compromises. First, to obtain such a rate of false positives, a higher rate of false negatives was accepted: 81 % of the grids visually considered as valid were indeed selected. Second, the microscope illumination should be homogeneous and properly set to operate with a good contrast: exposure time and illumination should be sufficiently high to achieve this goal, but not too high to avoid over-exposition of the camera. The saturation threshold of the camera has been set to 75%. This value is indicative but not critical as illustrated by the experimental results (see Section 5.2). At this magnification, the average time for the image processing is about 3s.

At medium magnification, the chain of algorithms detects edges of membranes, characterizes each region r and selects a list of targets. The computational time is about 15s. The quick ROI selection with the PED algorithm is about 2s. At this magnification, processing time is about 15s for the multi-resolution-based process, e.g. multi-resolution segmentation, contour validation, stacking representation, shape recognition, and ROI selection and about 2s for the PED ROI selection. In our example of Figure 11 two ROI are found in image 2, one in image 5 and none in image 9. Each ROI leads to one up to four high-magnification acquisitions.

At high magnification, the average time for image processing corresponds to the computation of the Fourier Transforms for the estimation of the power spectra and the diffraction peak identification. This treatment takes approximately one second. 98 % of the Fourier Transforms were properly automatically classified in terms of diffraction peaks. The false classifications are mainly due to bad-quality crystals or crystals presenting diffraction peaks with a SNR below the detection threshold (fixed by default to 3.5).

Table 1, second row, presents the average times of image processing for each magnification. Regarding the size of the images and the application, a relatively fast processing is available for on-line TEM image processing and target selection. Execution of the physical commands by the microscope (Table 1, first row) takes more time. The proposed strategy appears therefore to be well adapted for such controls.

Other strategies could also have been considered. For instance one could acquire all the images at low magnification, then the ones at medium magnification, and at last the ones at high magnification. However this strategy has been discarded

for a number of reasons. First, the low reliability and reproducibility of the stage movements: when moving to a targeted position, it seems better to increase the magnification immediately to the target without moving the stage, as the positioning error tends to get higher when the stage has been moved too much in between. Second, the low flexibility in the stopping commands such as stopping the processing of a grid when a satisfying amount of crystals has been found.

Conclusion

Table 2 shows the time and the number of images acquired at each magnification for a several runs. The overall time of a run directly depends on the amount of objects in the images, but also on conditions like the maximum number of low-magnification images to be acquired, the number of grid squares to analyze at medium magnification, or the maximum number of ROI for each medium-magnification image, (set by default to 20, 20, and 8 respectively).

Figure 12 shows the last run of Table 3 in detail. For example, we can see that the carbon film is completely broken on grid 8, cassette 1. Only 20 low-magnification images have been acquired; it takes less than 10 minutes to process such a grid. However, when the grid was interesting, 20 suitable grid squares have been identified, and for each of the medium-magnification images, at most 8 ROI have been identified, each one corresponding to an acquisition at high magnification.

Finally, in order to reduce these times, several ways are possible, such as doing the stage displacement and launch a new image acquisition at the same time while the previous high-magnification image is processed (Fourier Transform computation). Moreover we notice that by optimizing Matlab code into C-compiled code, these standard times for image processing can be greatly reduced.

5.2 ROI selection at medium magnification

The ROI selection at medium magnification is a crucial step for the correct development of the automatic analysis of 2D-crystals Therefore, It has to be robust, quick and as close as possible to the choices that would make a biologist during a traditional analysis of the grid. This is shown on an example where the

automatic selections made by ANIMATED-TEM are compared with the decisions of an expert, in various acquisition conditions.

ROI selection

The selection procedure described by biologists has widely contributed to the choice of the parameters used in the automatic selection of the ROI.

1. Only the lowest-stacked regions are selected. Indeed, the diffraction pattern is easier to study on non-stacked objects.
2. The smallest regions are removed from the selection. In our tests, we considered that small regions (500nm, i.e. smaller than the field of view at high magnification) are less interesting for pattern identification.
3. Experience shows that the crystalline membranes often present some linear edges. The general appearance of a membrane is thus a parameter that has to be considered.

Among all the segmented regions, only those that are considered non-stacked by the stacking algorithm and of size above 500nm are retained as targets. All other regions are discarded. It is then necessary to rank each of these regions in order to select the best ones. Each region is indexed both according to its size and the length of its linear edges. Regions are characterized by both indexes $L[Si_r] = n$ (for the size) and $L[Sh_r] = m$ (for the shape), with n,m $\in \mathbf{N}^*$, corresponding to the rank of the region compared to the other regions of the image. For the widest region $n = 1$; in the same way the region having the longest linear edge is characterized by $m = 1$. An average rank, $\bar{r}$, is deduced using:

$$\bar{r} = \frac{a \times L[Si_r] + b \times L[Sh_r]}{a + b},$$

where a and b are weights that can be used to adjust the importance of one of the parameters. ROI having the lowest $\bar{r}$ are considered as the best ones. By default, in our application, only the best two regions are used for acquisitions at high magnification. This limit can be modified by the user. Other criteria may be added to refine the choice of the ROI, considering for example a strong local contrast, meaning that a membrane contour is present rather than artifact-like stain.

Test conditions

Figure 13a shows an image acquired at medium magnification. We asked an expert to select the most appropriate areas at middle magnification to be checked for cristallinity at higher magnification. The result of this manual selection is presented in Figure 13b. Highly interesting regions are represented in black, interesting regions in gray. The main differences in this classification are the size and the shape of the regions. These two parameters come directly from the expert's manual segmentation. This image will be the reference image.

The conditions of image acquisition during a run are not always optimum, as a process to automatically set exposure time and illumination is not available yet. It is interesting to verify the robustness and the reproducibility of the selection by modifying their parameters in large ranges. Membranes of Figure 13a were thus acquired several times with various exposure times and illumination rates within realistic value ranges for that application. Table 3 shows the values of these parameters for each acquisition (acquisitions 1-11). In a second step, acquisitions have been made varying the magnifications (acquisitions 12-16)**,** then the stage position (acquisitions 17-22). Figure 14 shows each of these acquisitions on which the segmentations processed by ANIMATED-TEM are overlaid. The ROI are selected among these segmented regions. Several comments may already be made. First, it can be noted that the segmentation may vary depending on the acquisition conditions. Second, new elements may appear in the images depending on the magnification or the stage position. These parameters have not been considered during the classification done by the expert.

Results

The ROI have been selected on each of the 22 acquisitions of Figure 14. The results are presented in Figure 15. For each acquisition (abscissa), the percentage of ROI found by ANIMATED-TEM is represented according to the classification by the expert: first class in black, second class in dark gray, regions not selected by the expert in lighter gray, and regions not even present in the expert's image in pale gray (acquisition 12 to 22). Stars and little circles represent for each category the number of ROI found by ANIMATED-TEM, i.e. the number of non-stacked regions of over 500nm. Two stars for an acquisition correspond to the best two selected regions leading to acquisitions at high magnification. For example in

acquisition 7, 12 ROI have been found, 5 of them according to the first class of the expert (41,6%), 4 to the second one (33,3%) and 3 have not been retained by the expert (25%).

The main difference between first and second class lies in the size of the ROI. These two classes allow therefore to verify the crystallinity of a sample. We can notice that segmentation in regions within the different acquisitions is very variable, and what is considered by the expert as one sole zone can be broken down in several regions by ANIMATED-TEM.

When the acquisition parameters change for the same location (acquisition 1-11), we notice that in average 80% of the selections made by ANIMATED-TEM correspond to the selection of the expert. Moreover, if we only consider the two retained regions, only one of the ROI of acquisition 11 does not match with a choice of the expert, and for this acquisition the experimental conditions are far off the nominal values (Table 3). In 64% of cases, both selected targets match with regions of first class of the expert and in 91% of cases they are part of the choice of the expert (first or second class).

The goal of the application is to validate experiences of 2D crystallization. If the experimental protocol is correct, there will be plenty of occasions to observe crystalline membranes on the grid. Consequently, even if a few high-magnification acquisitions are useless because of a wrong choice of targets, it will not have a dramatic effect on the final result. There will be statistically enough observations allowing the characterization of the studied experimental protocol.

When the magnification is changed or when the stage is moved (acquisitions 12 to 22), the elements composing the image are not the same anymore. Yet the selection of the targets remains relevant. Except for acquisition 12 where the membrane we used as reference is too small and less interesting than other objects within the image, many regions being identified as interesting by the expert also appeared to be so by ANIMATED-TEM.

Conditions of acquisition have to be as good as possible to allow image processing tools to be efficient. Despite this, ANIMATED-TEM is capable of selecting ROI in a very robust manner, according to what a biologist expert would do, even when the conditions are not optimal.

Conclusion

In this article we have presented the first fully automated system for sample analysis without human intervention. In recent months, several test runs have been made, where about 1500 grids have been analyzed automatically, confirming the efficiency of the overall system. The image processing time is much less than the microscope control commands and can easily be optimized in future development. The proposed control strategy handling the acquisition procedure achieves the processing of a grid in an average of 34 minutes.

This first success of a full TEM automation opens the way for the development of image processing tools for electron microscopy.

Acknowledgments – This work was supported by the EU 6th framework (HT3DEM, LSHG-CT-2005-018811). Françoise Erne-Brand is warmly acknowledged for sample preparations and data acquisitions on the T12 at C-Cina.

References

[1] Suloway, C., Pulokas, J., Fellmann, D., Cheng, A., Guerra, F., Quispe, J., Stagg, S., Potter, C. S., and Carragher, B. O.: Automated molecular microscopy: The new Leginon system. Journal of Structural Biology, vol. 151, pp. 41-60, (2005).

[2] Zhang, J., Nakamura, N., Shimizu, Y., Liang, N., Liu, X., Jakana, J., Marsh, M. P., Booth, C. R., Shinkawa, T., Nakata, M., and Chiu, W.: JADAS: A customizable automated data acquisition system and its application to ice-embedded single particles. Journal of Structural Biology, vol. 165, pp. 1-9, (2009).

[3] Nickell, S., Förster, F., Linaroudis, A., Del Net, W., Beck, F., Hegerl, R., Baumeister, W., and Plitzko, J. M.: TOM software toolbox: acquisition and analysis for electron tomography. Journal of Structural Biology, vol. 149, pp. 227-234, (2005).

[4] Potter, C. S., Pulokas, J., Smith, P., Suloway, C., and Carragher, B.: Robotic grid loading system for a transmission electron microscope. Journal of Structural Biology, vol. 146, pp. 431-440, (2004).

[5] Lefman, J., Morrison, R., and Subramaniam, S.: Automated 100-position specimen loader and image acquisition system for transmission electron microscopy. Journal of Structural Biology, vol. 158, pp. 318-326, (2007).

[6] Coudray, N., Hermann, G., Caujolle-Bert, D., Karathanou, A., Erne-Brand, F., Buessler, J.-L., Daum, P., Plitzko, J., Chami, M., Mueller, U., Kihl, H., Urban, J.-P., Engel, A., and Rémigy, H.-W.: Automated

Screening of 2D Crystallization Trials Using Transmission Electron Microscopy: A High-Throughput Tool-Chain for Sample Preparation and Microscopic Analysis. (submitted to Journal of Structural Biology, July 2010).

[7] Koster, A. J., Chen, H., Sedat, J. W., and Agard, D. A.: Automated microscopy for electron tomography. Ultramicroscopy, vol. 46, pp. 207-227, (1992).

[8] Fan, G. Y., Mercurio, P. J., Young, S. J., and Ellisman, M. H.: Telemicroscopy. Ultramicroscopy, vol. 52, pp. 499-503, (1993).

[9] Kisseberth, N., Whittaker, M., Weber, D., Potter, C. S., and Carragher, B. O.: emScope: a tool kit for control and automation of a remote electron microscope. Journal of Structural Biology, vol. 120, pp. 309-319, (1997).

[10] Fung, J. C., Liu, W., Ruijter, W. J. d., Chen, H., Abbey, C. K., Sedat, J. W., and Agard, D. A.: Toward fully automated high-resolution electron tomography. Journal of Structural Biology, vol. 116, pp. 181-189, (1996).

[11] Dierksen, K., Typke, D., Hegerl, R., Walz, J., Sackmann, E., and Baumeister, W.: 3-Dimensional Structure of Lipid Vesicles Embedded in Vitreous Ice and Investigated by Automated Electron Tomography. Biophysical Journal, vol. 68, pp. 1416-1422, (1995).

[12] Mastronarde, D. N.: Automated electron microscope tomography using robust prediction of specimen movements. Journal of Structural Biology, vol. 152, pp. 36-51, (2005).

[13] Oostergetel, G. T., Keegstra, W., and Brisson, A.: Automation of specimen selection and data acquisition for protein electron crystallography. Ultramicroscopy, vol. 74, pp. 47-59, (1998).

[14] Anderson, J. R., Jones, B. W., Yang, J.-H., Shaw, M. V., Watt, C. B., Koshevoy, P., Spaltenstein, J., Jurrus, E., UV, K., Whitaker, R. T., Mastronarde, D., Tasdizen, T., and Marc, R. E.: A Computational Framework for Ultrastructural Mapping of Neural Circuitry. Plos Biology, vol. 7, pp. 493-512, (2009).

[15] Baker, T. S. and Cheng, R. H.: A model-based approach for determining orientations of biological macromolecules imaged by cryoelectron microscopy. Journal of Structural Biology, vol. 116, pp. 120-130, (1996).

[16] Nicholson, W. V. and Glaeser, R. M.: Automatic particle detection in electron microscopy. Journal of Structural Biology, vol. 133, pp. 90-101, (2001).

[17] Suloway, C., Shi, J., Cheng, A., Pulokas, J., Carragher, B., Potter, C. S., Zheng, S. Q., Agard, D. A., and Jensen, G. J.: Fully automated, sequential tilt-series acquisition with Leginon. Journal of Structural Biology, vol. 167, pp. 11-18, (2009).

[18] Zheng, S. Q., Keszthelyi, B., Branlund, E., Lyle, J. M., Braunfeld, M. B., Sedat, J. W., and Agard, D. A.: UCSF tomography: An integrated software suite for real-time electron microscopic tomographic data collection, alignment, and reconstruction. Journal of Structural Biology, vol. 157, pp. 138-147, (2007).

[19] Shi, J., Williams, D. R., and Stewart, P. L.: A Script Assisted Microscopy (SAM) Package to Improve Data Acquisition Rates on FEI Tecnai Electron Microscopes equipped with Gatan CCD Cameras. Journal of Structural Biology, vol. 164, pp. 166-169, (2008).

[20] Lei, J. L. and Frank, J.: Automated acquisition of cryo-electron micrographs for single particle reconstruction on an FEI Tecnai electron microscope. Journal of Structural Biology, vol. 150, pp. 69-80, (2005).

[21] Stagg, S. M., Lander, G. C., Pulokas, J., Fellmann, D., Cheng, A., Quispe, J. D., Mallick, S. P., Avila, R. M., Carragher, B. O., and Potter, C. S.: Automated cryoEM data acquisition and analysis of 284 742 particles of GroEL. Journal of Structural Biology, vol. 155, pp. 470-481, (2006).

[22] Cheng, A., Leung, A., Fellmann, D., Quispe, J., Suloway, C., Pulokas, J., Carragher, B., and Potter, C. S.: Towards automated screening of two-dimensional crystals. Journal of Structural Biology, vol. 160, pp. 324-331, (2007).

[23] Hu, M., Vink, M., Kim, C., Derr, K., Koss, J., D'Amico, K., Cheng, A., Pulokas, J., Ubarretxena-Belandia, I., and Stokes, D.: Automated Electron Microscopy for Evaluating Two-dimensional Crystallization of Membrane Proteins. Journal of Structural Biology, vol. 171, pp. 102-110, (2010).

[24] Kylberg, G., Sintorn, I.-M., and Borgefors, G.: Towards Automated TEM for Virus Diagnostics: Segmentation of Grid Squares and Detection of Regions of Interest. Image Analysis, pp. 169-178, (2009).

[25] Karathanou, A., Coudray, N., Hermann, G., Buessler, J.-L., and Urban, J.-P.: Automatic TEM image analysis of membranes for 2D crystal detection, in Springer AEMB, Advances in Computational Biology. vol. 680, H. R. Arabnia, Ed., (2010).

[26] Coudray, N., Buessler, J.-L., and Urban, J.-P.: A robust thresholding algorithm for unimodal image histograms. Pattern Recognition Letters, vol. 31, pp. 1010-1019, (2010).

[27] Coudray, N., Buessler, J.-L., Kihl, H., and Urban, J.-P.: Multi-scale and first derivative analysis for edge detection in TEM images, in 4th International Conference on Image Analysis and Recognition (ICIAR 2007), Montréal, Canada, pp. 1005-1016, (2007).

[28] Karathanou, A., Buessler, J.-L., Kihl, H., and Urban, J.-P.: Detection of low contrasted membranes in electron microscope images: statistical contour validation, in Digital Imaging Sensors and Applications, Part of the Imaging Science and Technology/SPIE, 21th Annual Symposium on Electronic Imaging, San Jose, Cal, USA, (2009).

[29] Hermann, G., Karathanou, A., Buessler, J.-L., and Urban, J.-P.: Evaluation of membrane stacking in electron microscope images, in Digital Imaging Sensors and Applications, Part of the Imaging Science and Technology/SPIE, 21th Annual Symposium on Electronic Imaging, San Jose, Cal, USA, (2009).

[30] Karathanou, A., Buessler, J.-L., Kihl, H., and Urban, J.-P.: Background Extraction in Electron Microscope Images of Artificial Membranes, in 5th

IFIP conference on Artificial Intelligence Applications and Innovations, Thessaloniki, Greece, pp. 165-173, (2009).

[31] Hermann, G., Kihl, H., and Urban, J.-P.: Detection and Characterization of Vesicles in EM Images, in The 2010 International Conference on Bioinformatics and Computational Biology (Biocomp), Las Vegas, USA, (2010).

Figure Captions

Fig. 1 Selection (white squares) of valid membranes grid squares

Fig. 2 Structure of the image processing chain for medium-magnification images

Fig. 3 Illustrative example of an image processing chain for medium-magnification images. A/ Initial image; B/ Result of contour detection displayed on the initial image; C/ Segments to be removed (in red) after statistical analysis of the local contrasts; D/ Labeling of the stacking (lowest-stacked regions in red, bi-stacked regions in green; three-stacked regions in magenta; multi-stacked regions in cyan); E/ Labeling of the shapes of the contour (linear portions in red; circular portions in cyan; portions not associated with any of these two shapes in black)

Fig. 4 Detailed architecture of the microscope control and interaction with the TEM and the image processing computer

Fig. 5 Carousel GUI Left: visual and manual control of the state of the carousel; Right: pop up window to initialize the position of the 8 cassettes within the carousel

Fig. 6 Typical example of an automatic run scenario at 3 magnification levels. Selected grid squares appear in red at low magnification; Selected targets appear, at medium magnification, in yellow (PED method) and red (multi-resolution-based method); identified diffraction peaks appear in red ($4.5 \leq SNR$), blue ($4 \leq SNR < 4.5$) and green ($3.5 \leq SNR < 4$)

Fig. 1 Flowchart of the major steps of the scenario ($\sum MM$ is the amount of images acquired at medium magnification on the whole grid)

Fig. 8 Example of 20 low-magnification images acquired during a run; numbers show the order in which the images have been acquired; each image is processed immediately after its acquisition

Fig. 9 GUI to set the parameters for an automatic run (above), and two pop-up windows to select the grids to be analyzed (left), and to adjust the default parameters used by image processing algorithms (right)

Fig. 10 GUI to browse through the result and the corresponding pop-up window displaying statistical results for each of the grid analyzed

Fig. 11 Example of the chronology of events in an automatic run

Fig. 12 Pop-up window showing a summary of an automatic run executed with 96 grids

Fig. 13 a) Initial image at medium magnification and b) ROI selection by an expert

Fig. 14 Results of the automatic partition obtained on the same object acquired under different conditions

Fig. 15 Comparative results of the automated selection at medium magnification, for images acquired under different conditions

Figure 1

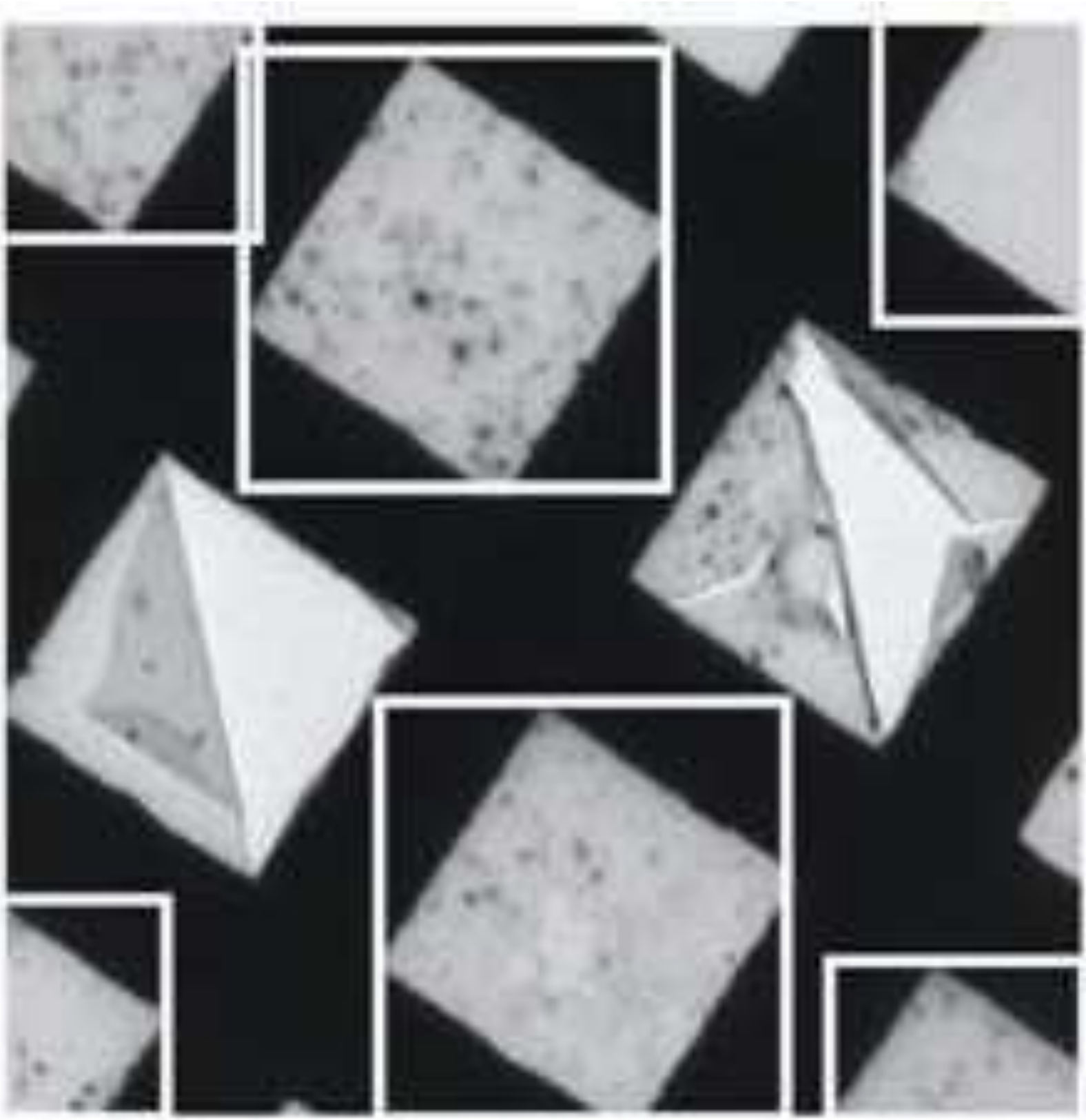

Figure 2

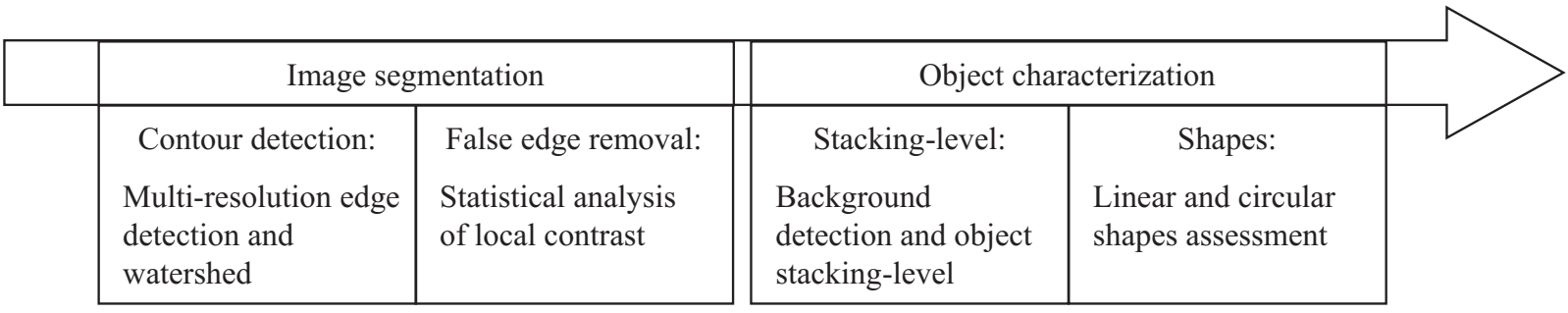
Image segmentation
Object characterization
Contour detection:
Multi-resolution edge detection and watershed
False edge removal:
Statistical analysis of local contrast
Stacking-level:
Background detection and object stacking-level
Shapes:
Linear and circular shapes assessment

Figure 3

Click here to download high resolution image

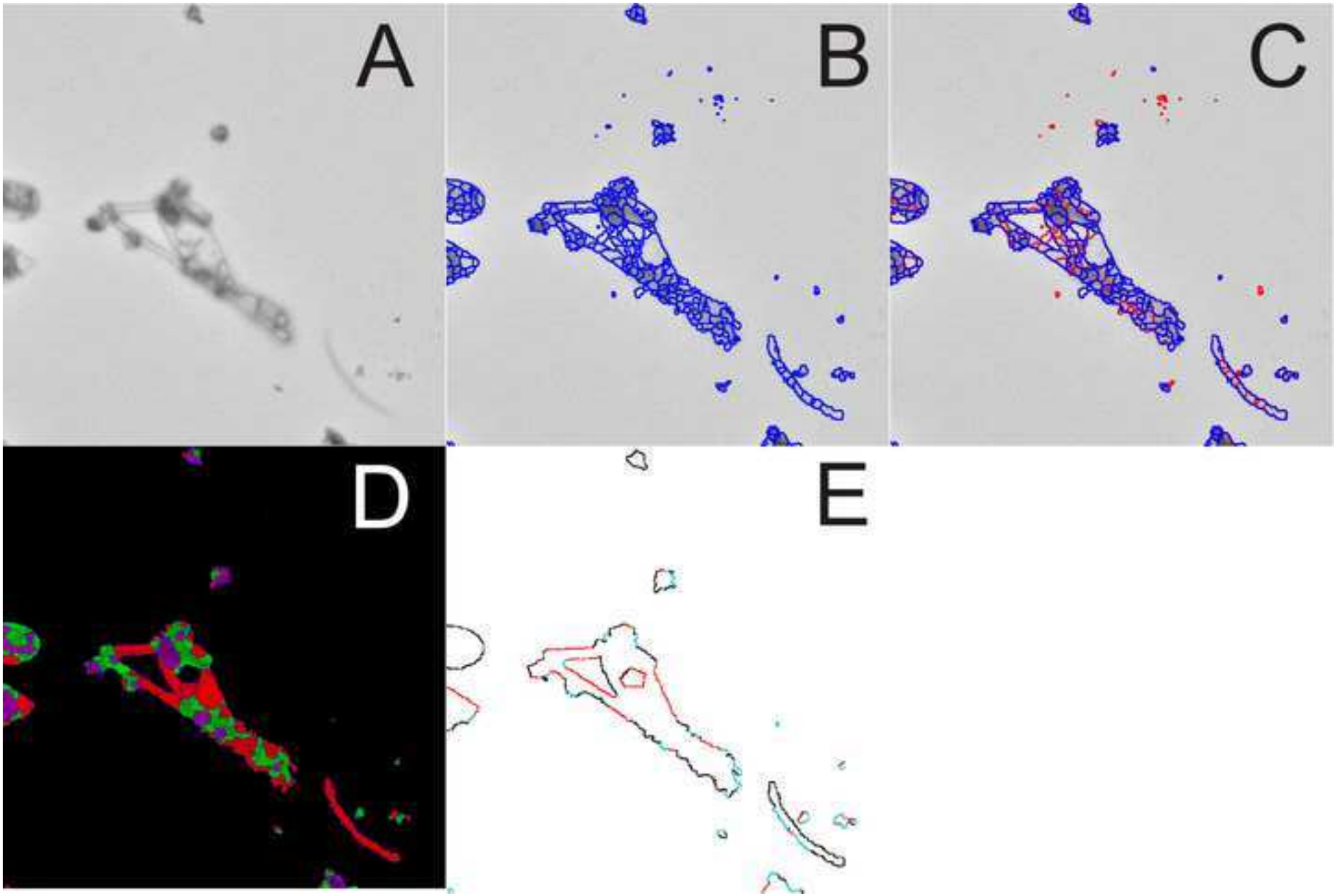

Figure 4

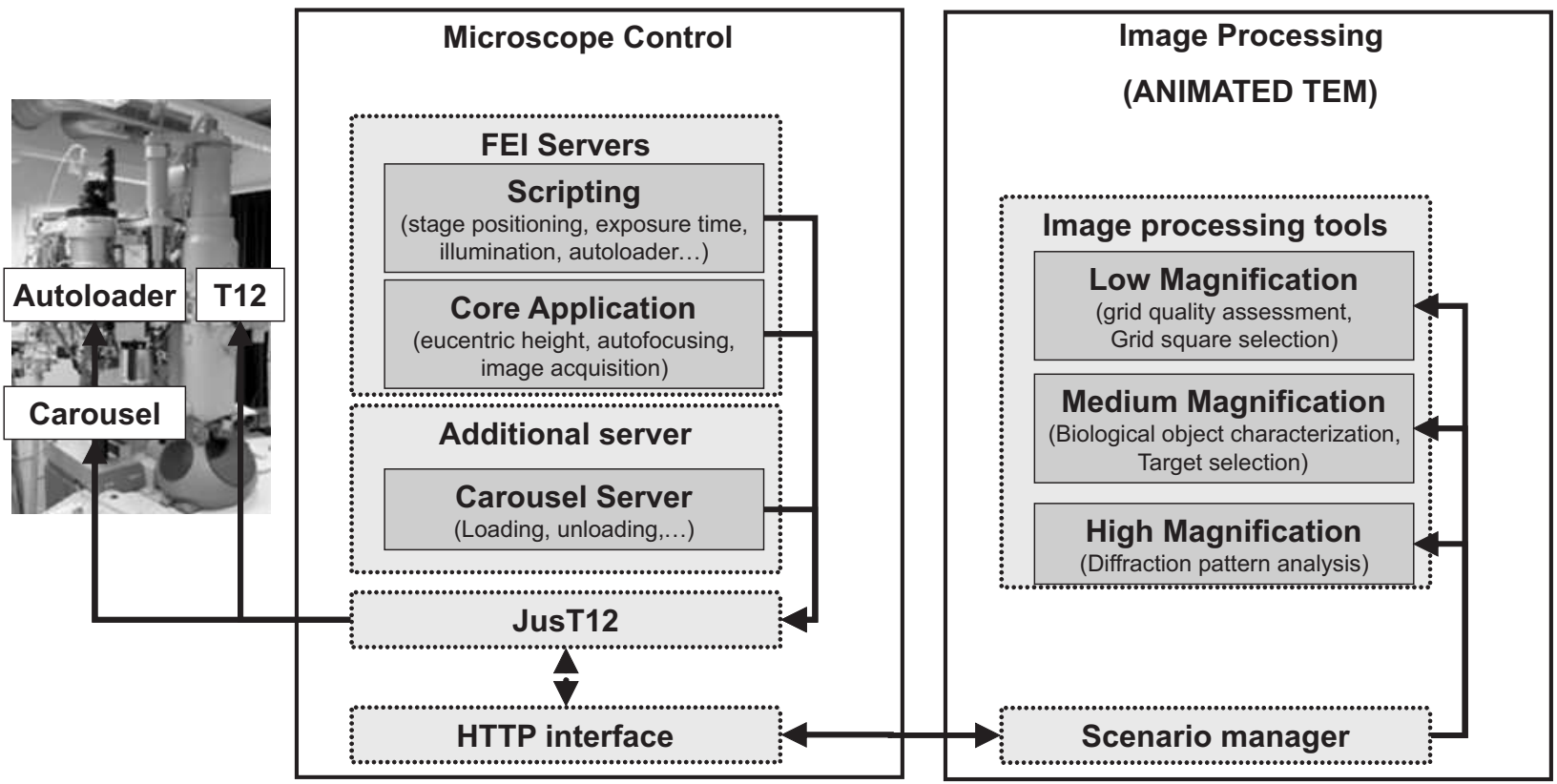
Microscope Control
Image Processing
(ANIMATED TEM)
Autoloader
T12
Carousel
FEI Servers
Scripting
(stage positioning, exposure time, illumination, autoloader…)
Core Application
(eucentric height, autofocusing, image acquisition)
Additional server
Carousel Server
(Loading, unloading,…)
JusT12
HTTP interface
Image processing tools
Low Magnification
(grid quality assessment, Grid square selection)
Medium Magnification
(Biological object characterization, Target selection)
High Magnification
(Diffraction pattern analysis)
Scenario manager

Figure 5

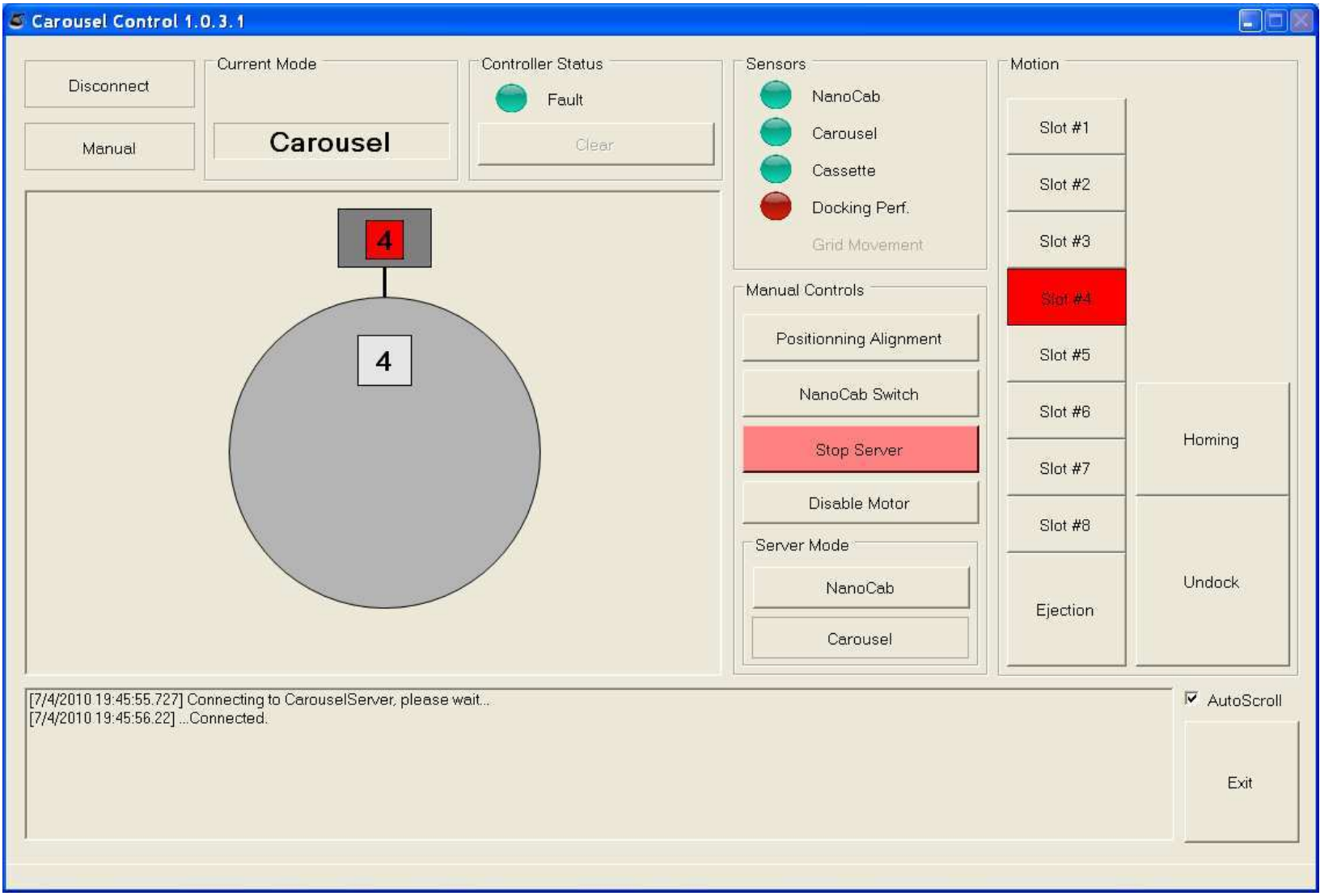
Carousel Control 1.0.3.1
Disconnect
Manual
Current Mode
Carousel
Controller Status
Fault
Clear
Sensors
NanoCab
Carousel
Cassette
Docking Perf.
Grid Movement
Motion
Slot #1
Slot #2
Slot #3
Slot #4
Slot #5
Slot #6
Slot #7
Slot #8
Ejection
Homing
Undock
4
4
Manual Controls
Positionning Alignment
NanoCab Switch
Stop Server
Disable Motor
Server Mode
NanoCab
Carousel
[7/4/2010 19:45:55.727] Connecting to CarouselServer, please wait...
[7/4/2010 19:45:56.22] ...Connected.
AutoScroll
Exit

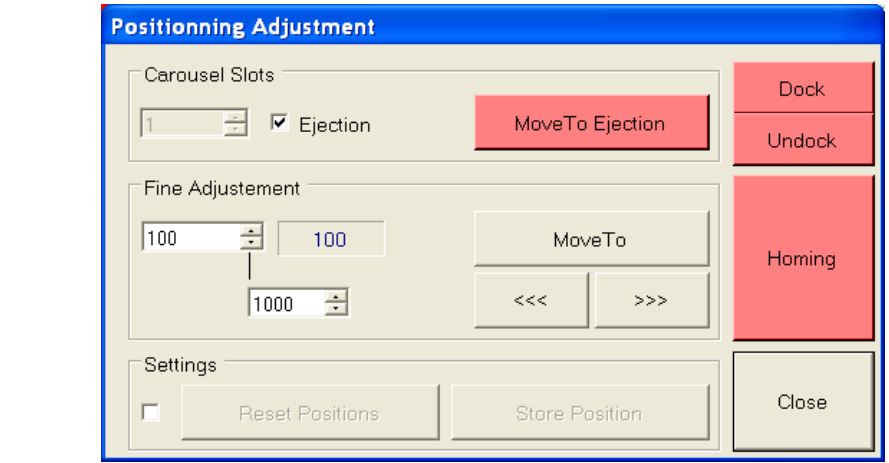
Positionning Adjustment
Carousel Slots
1
Ejection
MoveTo Ejection
Dock
Undock
Fine Adjustement
100
100
MoveTo
1000
<<<
>>>
Homing
Settings
Reset Positions
Store Position
Close

Figure 6

Low Magnification

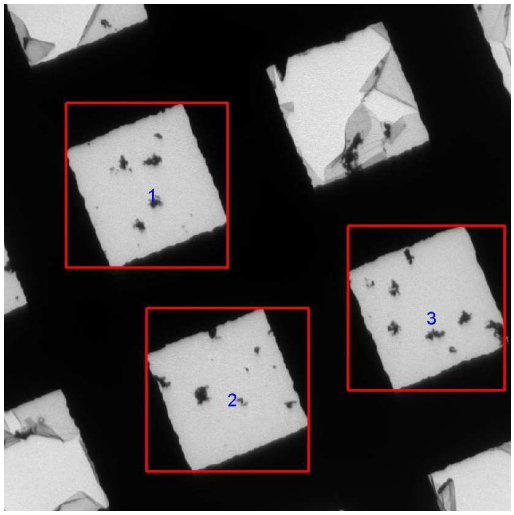

For all selected grid squares

Medium Magnification

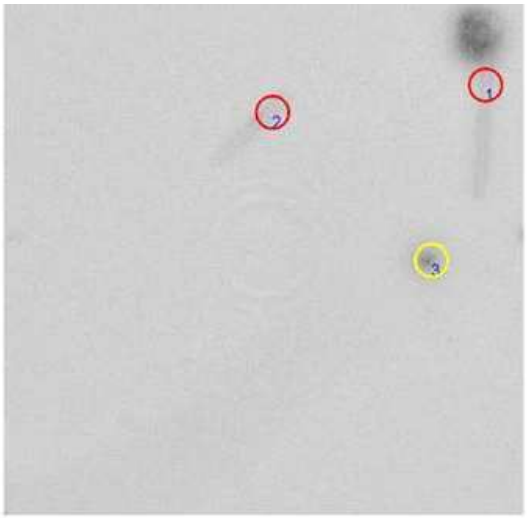

For all selected ROIs

High Magnification

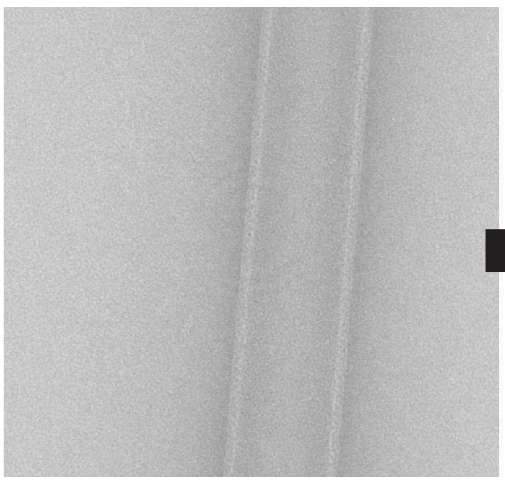

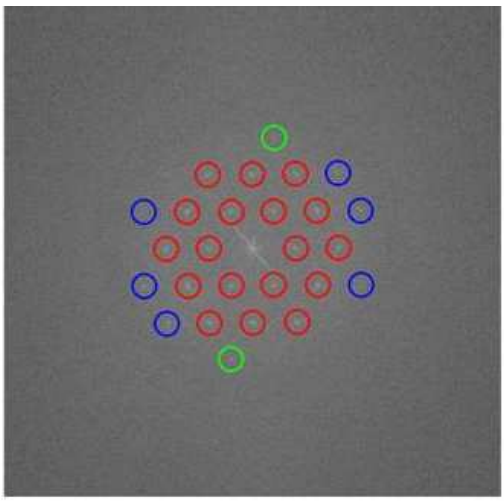

Figure 7

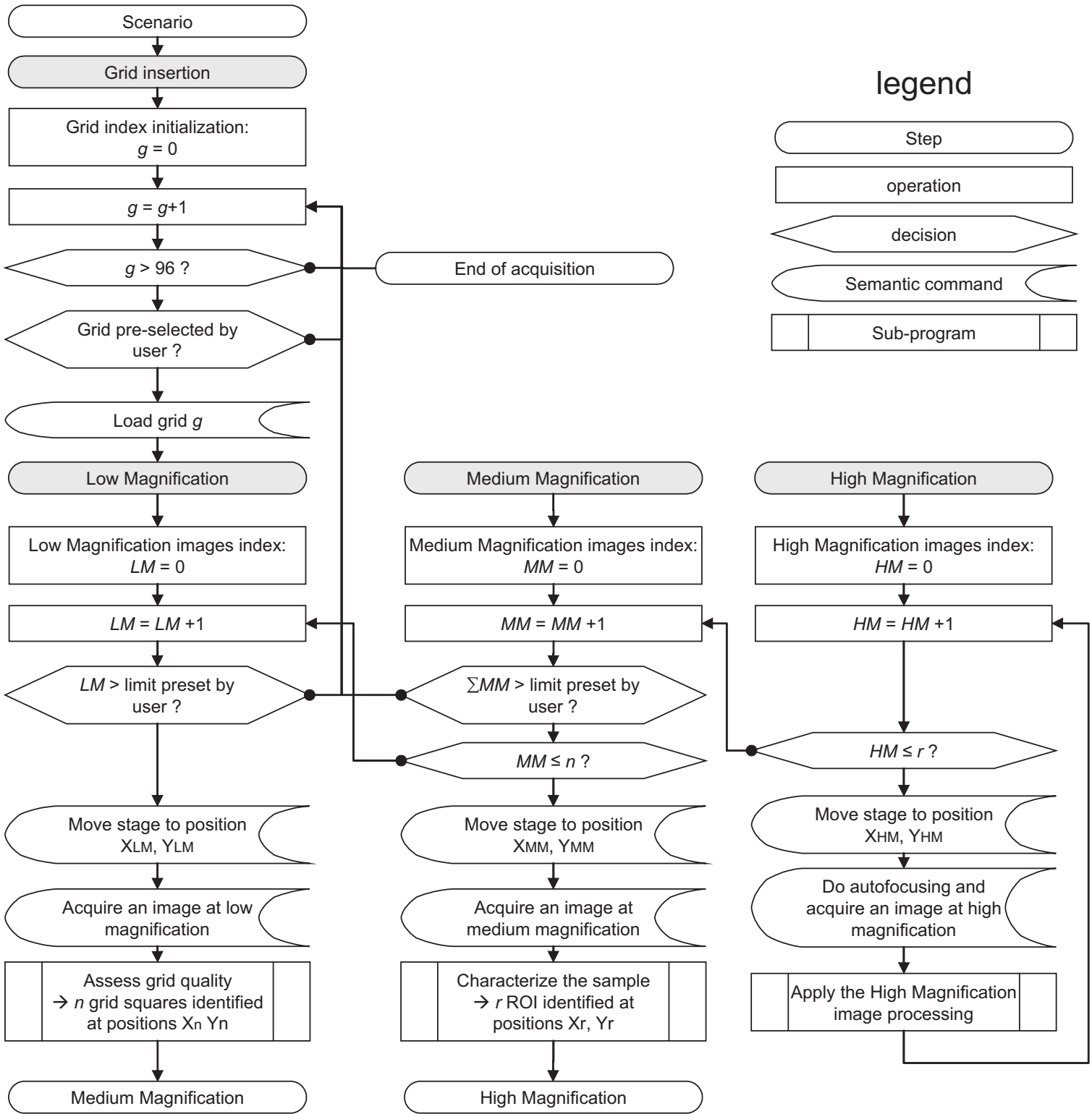
Scenario
Grid insertion
Grid index initialization:
g = 0
g = g+1
g > 96 ?
End of acquisition
Grid pre-selected by user ?
Load grid g
Low Magnification
Low Magnification images index:
LM = 0
LM = LM +1
LM > limit preset by user ?
Move stage to position XLM, YLM
Acquire an image at low magnification
Assess grid quality
→ n grid squares identified at positions Xn Yn
Medium Magnification
Medium Magnification
Medium Magnification images index:
MM = 0
MM = MM +1
∑MM > limit preset by user ?
MM ≤ n ?
Move stage to position XMM, YMM
Acquire an image at medium magnification
Characterize the sample
→ r ROI identified at positions Xr, Yr
High Magnification
High Magnification
High Magnification images index:
HM = 0
HM = HM +1
HM ≤ r ?
Move stage to position XHM, YHM
Do autofocusing and acquire an image at high magnification
Apply the High Magnification image processing
legend
Step
operation
decision
Semantic command
Sub-program

Figure 8

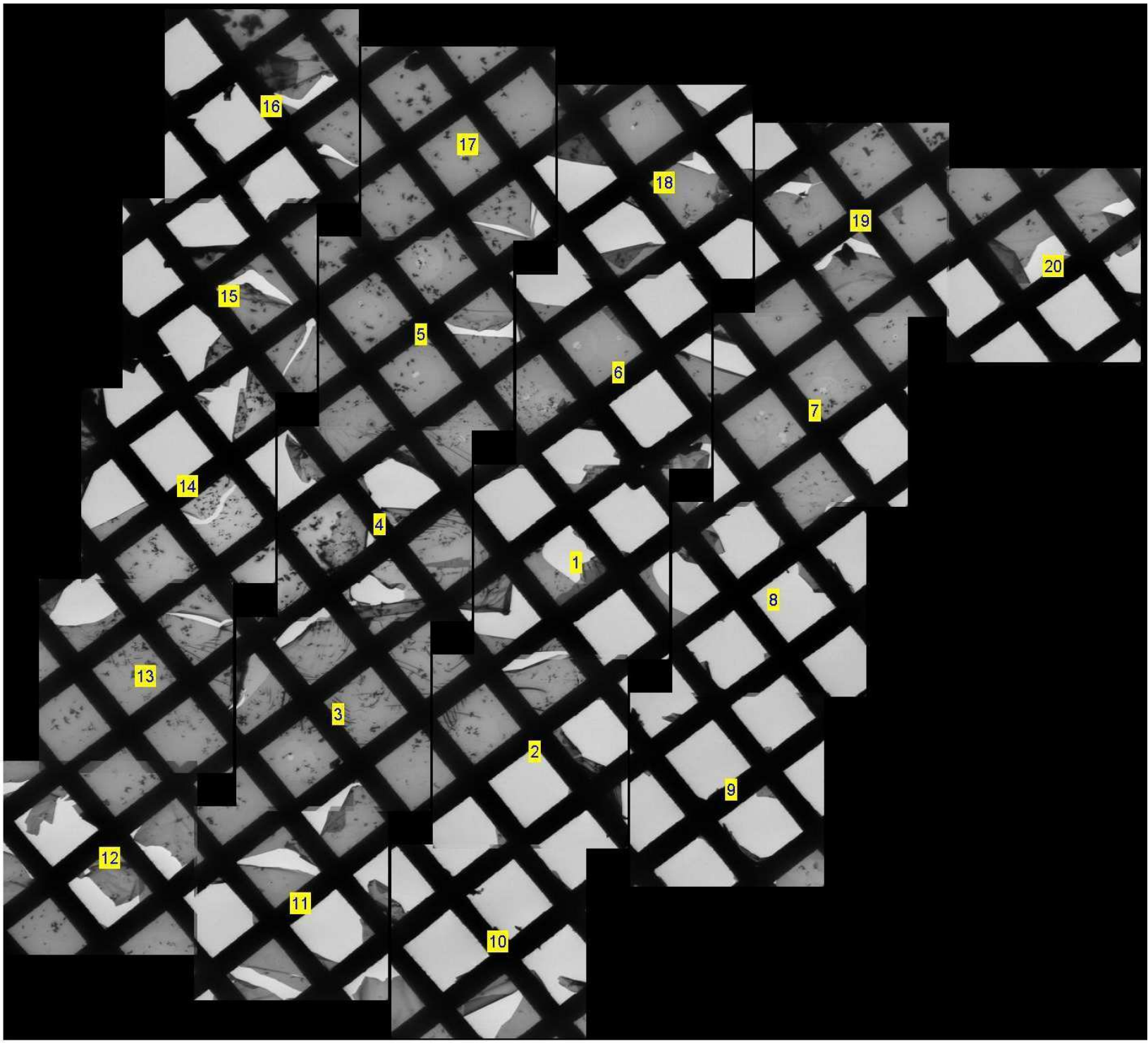

Figure 3

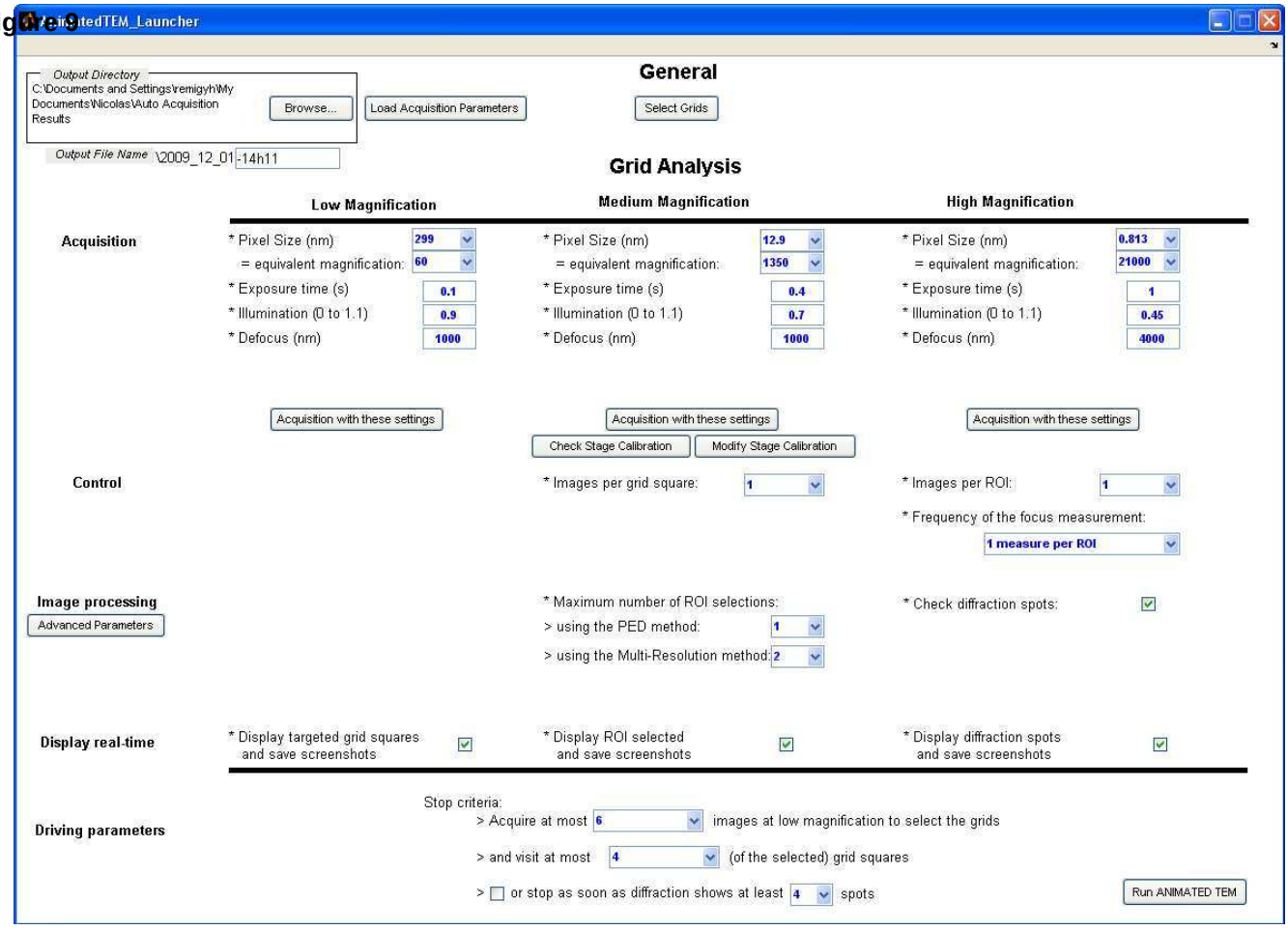
AnimatedTEM_Launcher
Output Directory
C:\Documents and Settings\remigyh\My Documents\Nicolas\Auto Acquisition Results
Browse...
Load Acquisition Parameters
General
Select Grids
Output File Name \2009_12_01-14h11
Grid Analysis
Low Magnification
Medium Magnification
High Magnification
Acquisition
* Pixel Size (nm) 299
= equivalent magnification: 60
* Exposure time (s) 0.1
* Illumination (0 to 1.1) 0.9
* Defocus (nm) 1000
* Pixel Size (nm) 12.9
= equivalent magnification: 1350
* Exposure time (s) 0.4
* Illumination (0 to 1.1) 0.7
* Defocus (nm) 1000
* Pixel Size (nm) 0.813
= equivalent magnification: 21000
* Exposure time (s) 1
* Illumination (0 to 1.1) 0.45
* Defocus (nm) 4000
Acquisition with these settings
Acquisition with these settings
Check Stage Calibration
Modify Stage Calibration
Acquisition with these settings
Control
* Images per grid square: 1
* Images per ROI: 1
* Frequency of the focus measurement:
1 measure per ROI
Image processing
Advanced Parameters
* Maximum number of ROI selections:
> using the PED method: 1
> using the Multi-Resolution method: 2
* Check diffraction spots:
Display real-time
* Display targeted grid squares and save screenshots
* Display ROI selected and save screenshots
* Display diffraction spots and save screenshots
Driving parameters
Stop criteria:
> Acquire at most 6 images at low magnification to select the grids
> and visit at most 4 (of the selected) grid squares
> or stop as soon as diffraction shows at least 4 spots
Run ANIMATED TEM

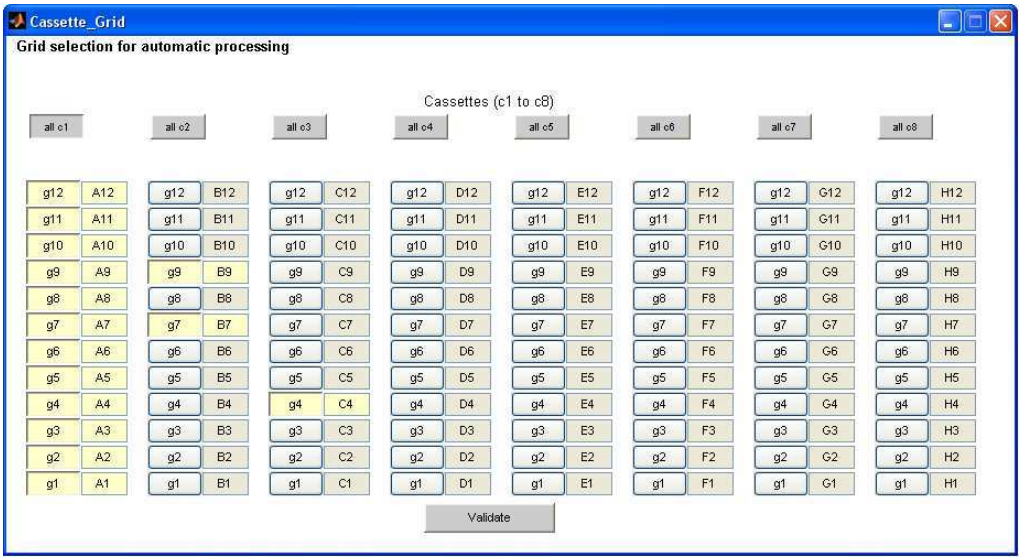
Cassette_Grid
Grid selection for automatic processing
Cassettes (c1 to c8)
all c1
all c2
all c3
all c4
all c5
all c6
all c7
all c8
Validate

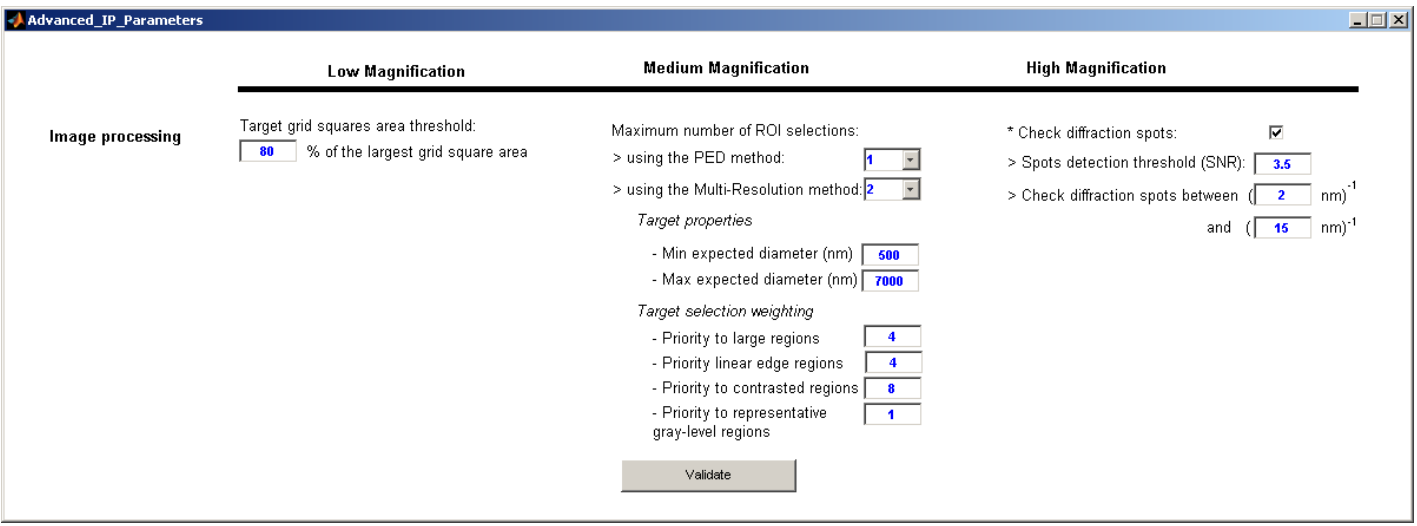
Advanced_IP_Parameters
Low Magnification
Medium Magnification
High Magnification
Image processing
Target grid squares area threshold:
80 % of the largest grid square area
Maximum number of ROI selections:
> using the PED method: 1
> using the Multi-Resolution method: 2
Target properties
- Min expected diameter (nm) 500
- Max expected diameter (nm) 7000
Target selection weighting
- Priority to large regions 4
- Priority linear edge regions 4
- Priority to contrasted regions 8
- Priority to representative gray-level regions 1
* Check diffraction spots:
> Spots detection threshold (SNR): 3.5
> Check diffraction spots between (2 nm)-1
and (15 nm)-1
Validate

Figure 10

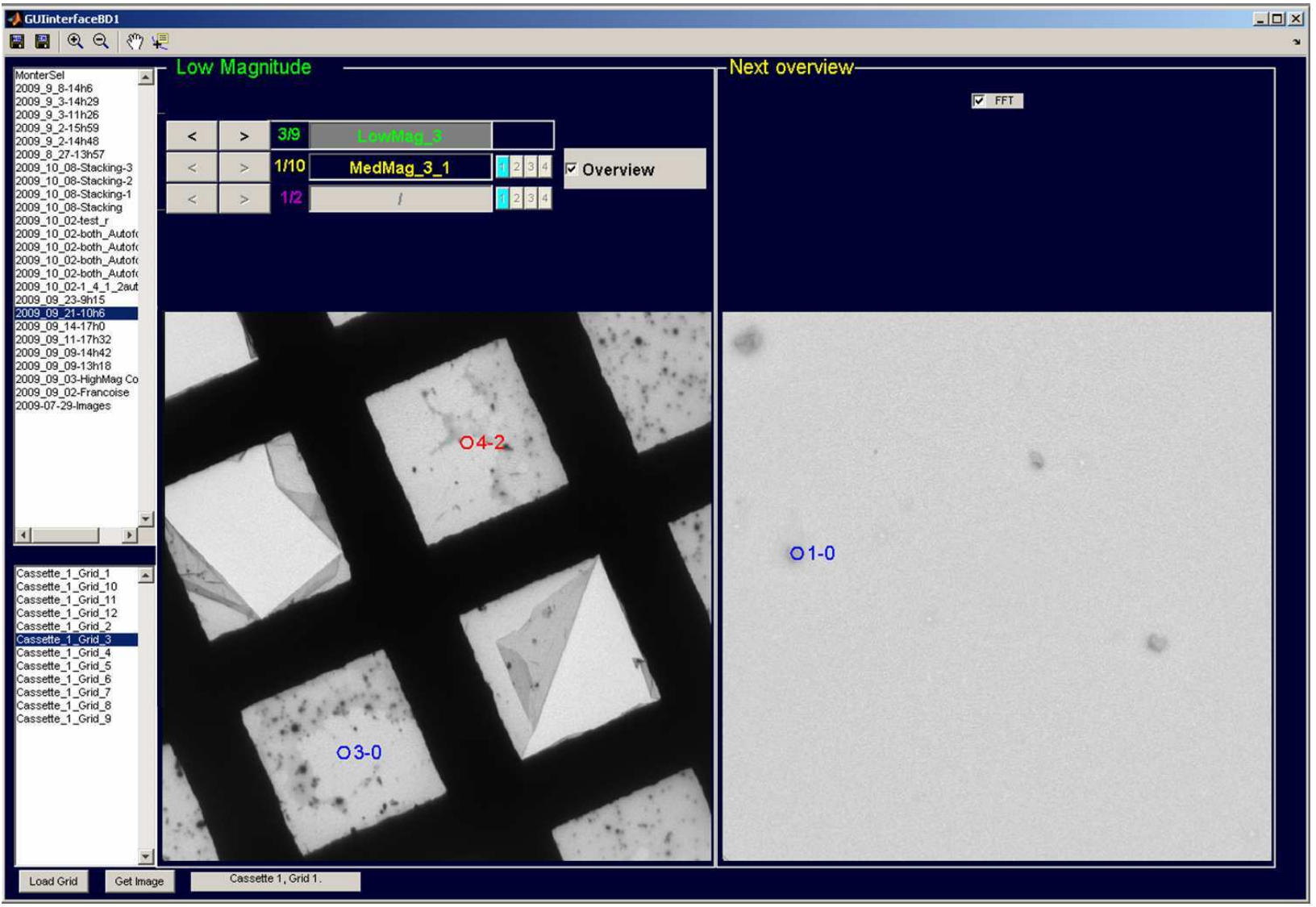
GUIinterfaceBD1
Low Magnitude
Next overview
FFT
MonterSel
2009_9_8-14h6
2009_9_3-14h29
2009_9_3-11h26
2009_9_2-15h59
2009_9_2-14h48
2009_8_27-13h57
2009_10_08-Stacking-3
2009_10_08-Stacking-2
2009_10_08-Stacking-1
2009_10_08-Stacking
2009_10_02-test_r
2009_09_23-9h15
2009_09_21-10h6
2009_09_14-17h0
2009_09_11-17h32
2009_09_09-14h42
2009_09_09-13h18
2009_09_03-HighMag Co
2009_09_02-Francoise
2009-07-29-Images
3/9
LowMag_3
1/10
MedMag_3_1
1/2
Overview
4-2
1-0
3-0
Cassette_1_Grid_1
Cassette_1_Grid_10
Cassette_1_Grid_11
Cassette_1_Grid_12
Cassette_1_Grid_2
Cassette_1_Grid_3
Cassette_1_Grid_4
Cassette_1_Grid_5
Cassette_1_Grid_6
Cassette_1_Grid_7
Cassette_1_Grid_8
Cassette_1_Grid_9
Load Grid
Get Image
Cassette 1, Grid 1.

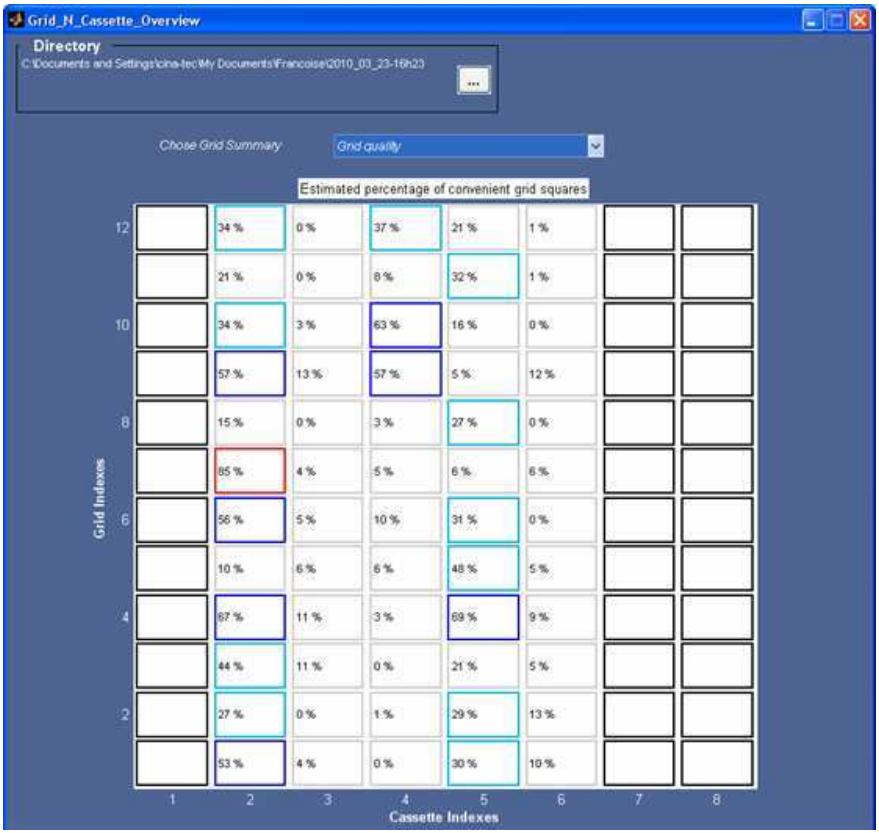
Grid_N_Cassette_Overview
Directory
Chose Grid Summary
Grid quality
Estimated percentage of convenient grid squares
Grid Indexes
Cassette Indexes

Figure 11

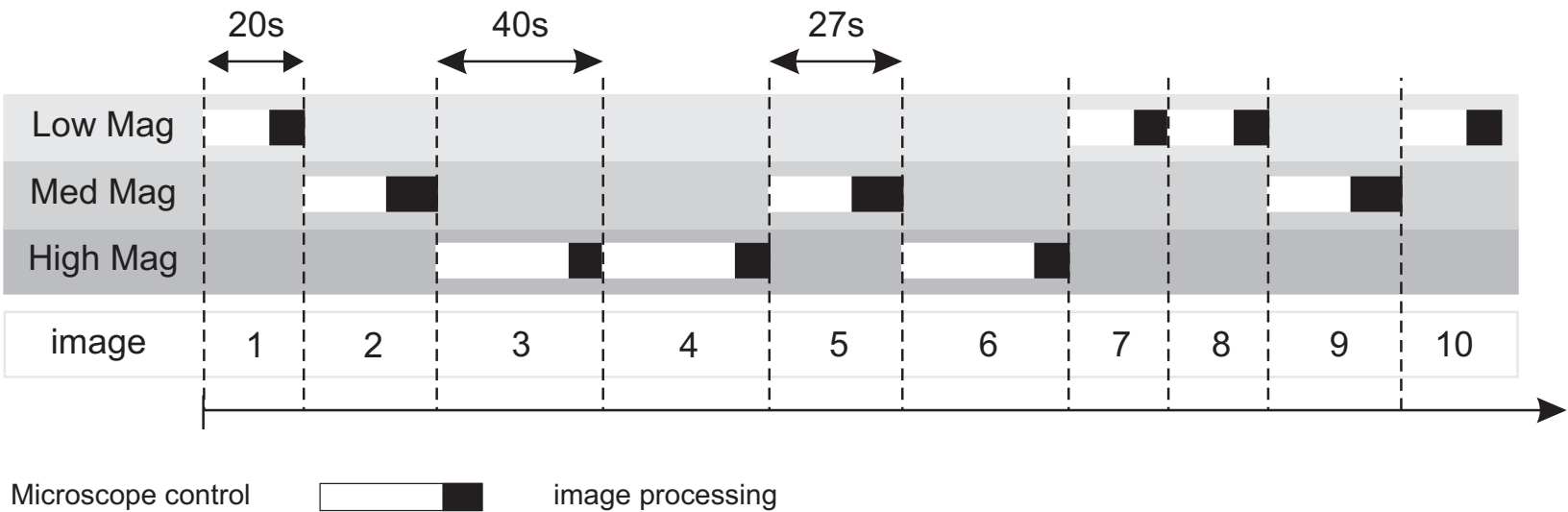
20s
40s
27s
Low Mag
Med Mag
High Mag
image
1
2
3
4
5
6
7
8
9
10
Microscope control
image processing

Figure 12


Grid_N_Cassette_Overview
Directory
C:\Documents and Settings\cina-tec\My Documents\Francoise\2010_07_19-96g_run0
...
Chose Grid Summary
Nbr of images and Processing Time
6234 images (1254 LM, 1751 MM, 3229 HM), over 96 grids, in 8 cassettes, in 2 days, 11h7'44"
Grid Indexes
Cassette Indexes
12
10
8
6
4
2
1
2
3
4
5
6
7
8
9+20+87=116 70min56
20+5+5=30 13min49
14+20+44=78 41min50
7+20+45=72 42min3
20+7+24=51 27min25
12+20+33=65 35min58
10+20+13=43 22min5
20+3+10=33 15min45
7+20+124=151 96min24
13+20+9=42 21min6
12+20+14=46 22min44
8+20+47=75 42min17
16+20+49=85 51min33
20+20+6=46 20min28
14+20+9=43 20min39
16+20+11=47 22min29
9+20+97=126 79min28
20+5+5=30 14min13
10+20+49=79 43min2
9+20+35=64 37min9
19+20+58=97 55min58
20+9+14=43 20min55
9+20+7=36 18min6
14+20+16=50 24min59
11+20+92=123 73min34
20+20+20=60 30min25
9+20+30=59 33min25
15+20+16=51 26min0
6+20+33=59 35min9
20+8+14=42 21min53
10+20+13=43 22min7
11+20+22=53 27min44
20+0+0=20 8min19
12+20+30=62 35min38
14+20+19=53 27min8
20+16+12=48 23min16
10+20+12=42 22min12
10+20+22=52 27min55
20+13+5=38 16min52
20+14+17=51 25min10
7+20+19=46 25min45
11+20+12=43 21min56
9+20+10=39 19min21
15+20+50=85 48min50
9+20+33=62 36min24
20+16+42=78 43min48
9+20+1=30 13min14
13+20+20=53 27min11
7+20+91=118 71min54
10+20+25=55 30min11
8+20+21=49 26min53
11+20+49=80 46min12
10+20+67=97 57min52
8+20+15=43 23min25
11+20+16=47 23min26
19+20+12=51 24min17
8+20+63=91 55min47
7+20+62=89 53min54
8+20+23=51 29min22
13+20+25=58 30min34
7+20+55=82 51min9
20+20+66=106 56min57
20+2+0=22 9min2
12+20+7=39 19min12
20+8+26=54 27min1
19+20+5=44 19min15
20+12+19=51 26min6
12+20+14=46 22min16
11+20+29=60 34min42
11+20+58=89 52min3
19+20+19=58 27min37
9+20+14=43 21min50
19+20+118=157 98min39
20+17+70=107 70min29
8+20+56=84 51min13
6+20+17=43 22min58
10+20+20=50 26min42
20+19+47=86 46min40
10+20+2=32 14min47
9+20+3=32 14min50
8+20+102=130 79min30
15+20+103=138 90min7
17+20+28=65 34min58
12+20+23=55 28min13
9+20+31=60 34min56
17+20+63=100 56min43
16+20+3=39 17min2
9+20+11=40 20min18
15+20+103=138 81min17
9+20+126=155 107min46
20+17+21=58 38min4
9+20+20=49 34min16
13+20+45=78 53min2
15+20+65=100 67min30
10+20+8=38 27min38
9+20+8=37 26min45

Figure 13

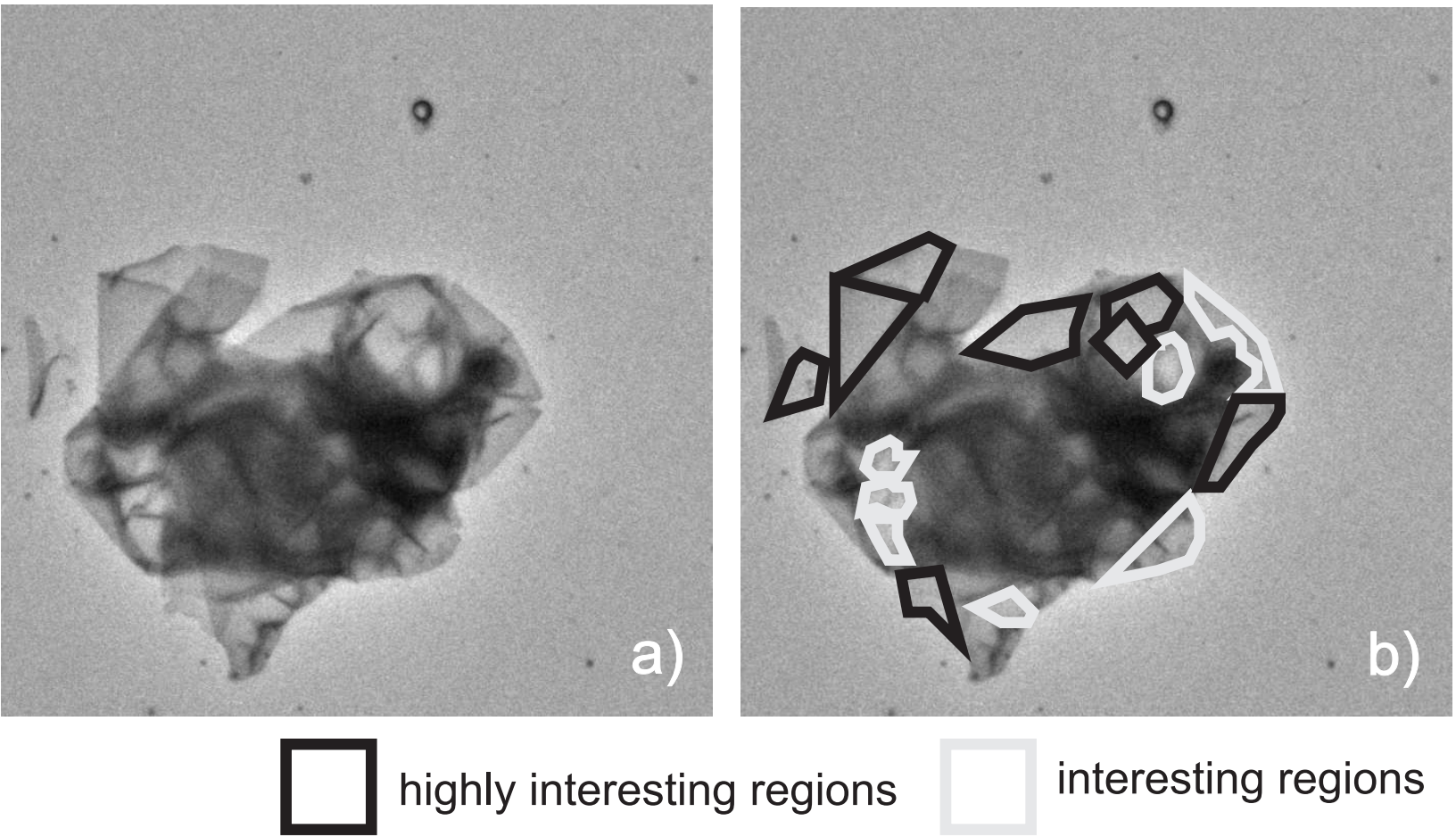

Figure 14

Click here to download high resolution image

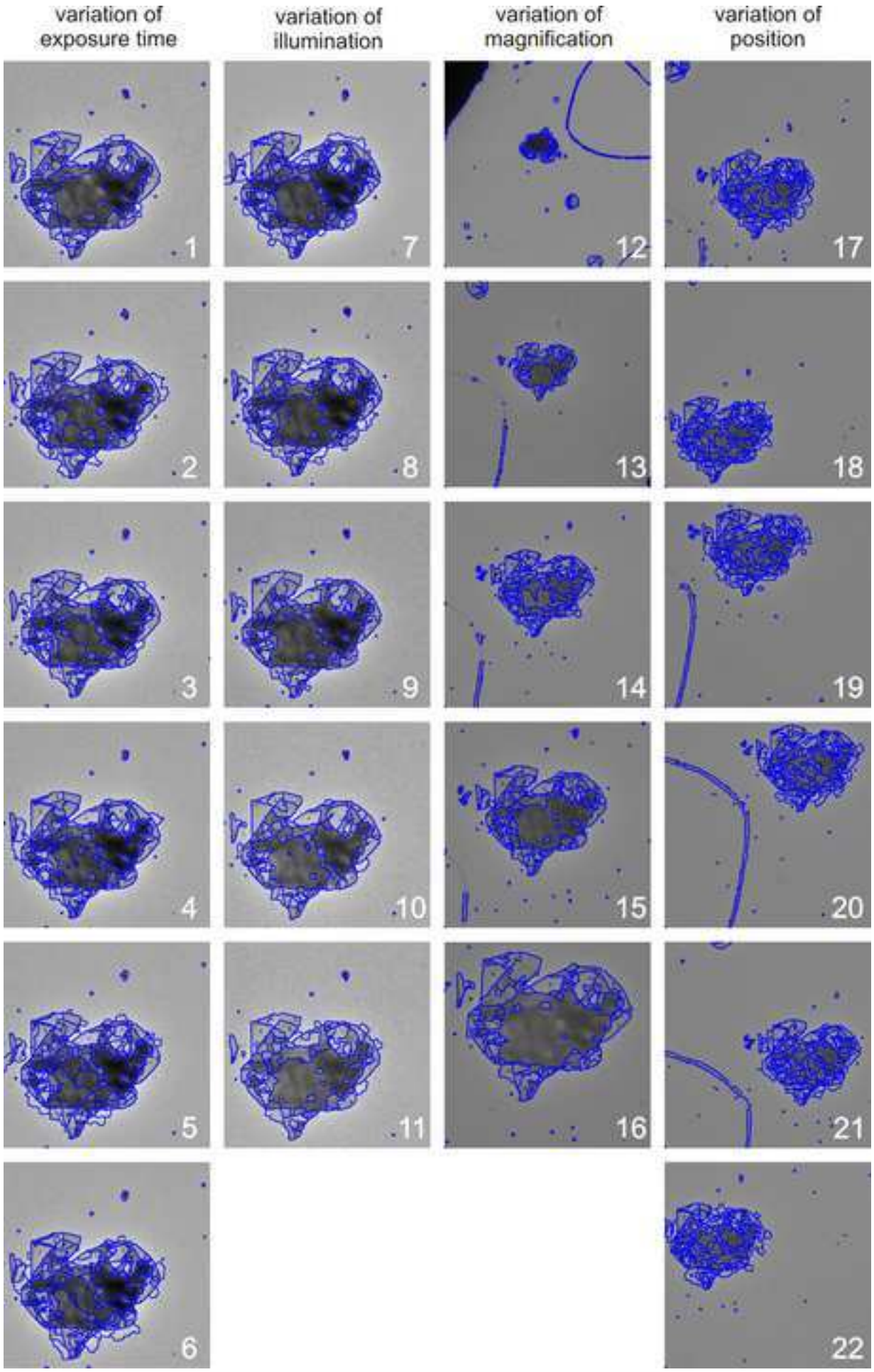

Figure 15

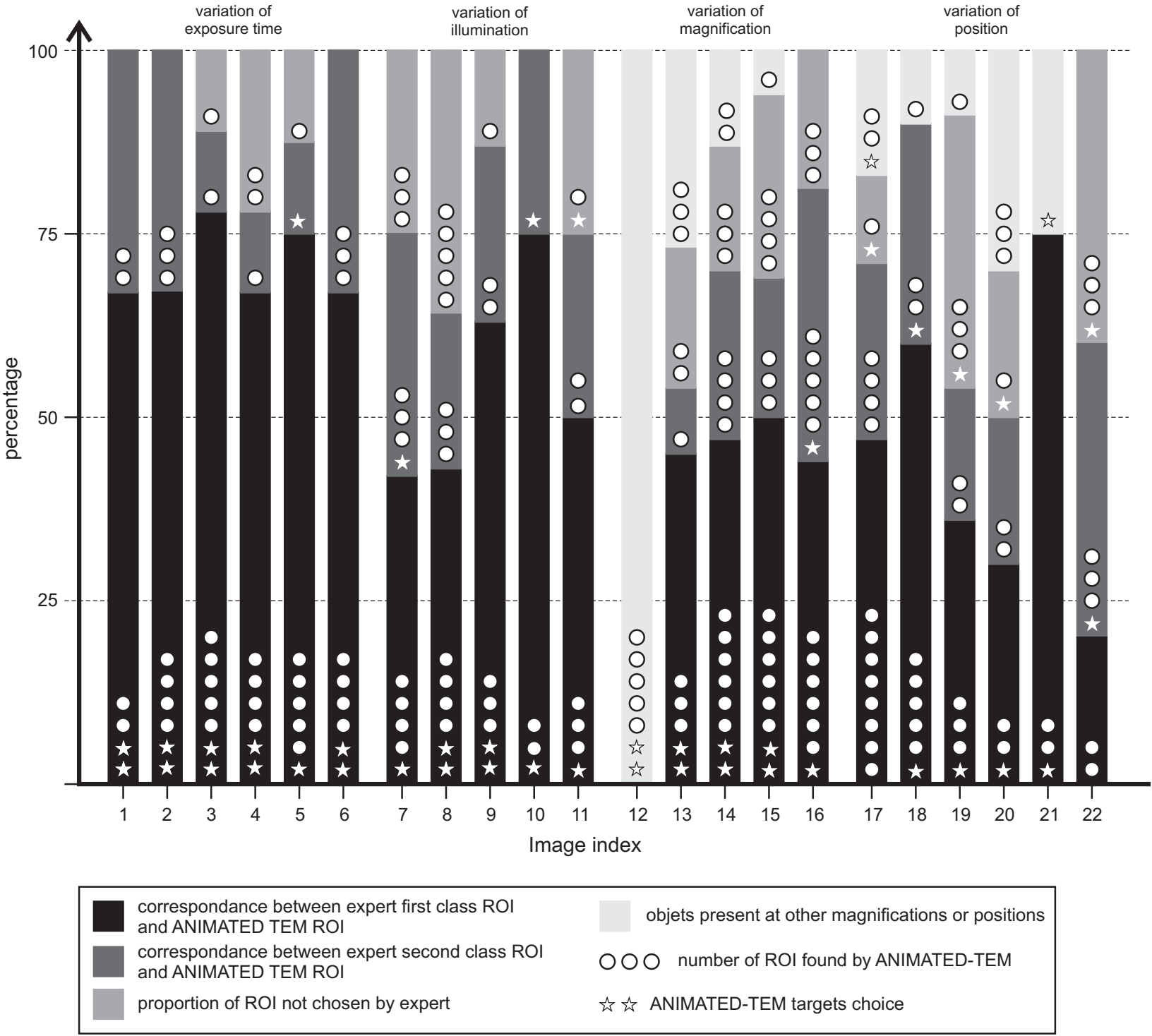
variation of exposure time
variation of illumination
variation of magnification
variation of position
100
75
50
25
percentage
1
2
3
4
5
6
7
8
9
10
11
12
13
14
15
16
17
18
19
20
21
22
Image index
correspondance between expert first class ROI and ANIMATED TEM ROI
correspondance between expert second class ROI and ANIMATED TEM ROI
proportion of ROI not chosen by expert
objets present at other magnifications or positions
number of ROI found by ANIMATED-TEM
ANIMATED-TEM targets choice

Table 1

Table 1 Average processing times

Magnification	Low Magnification	Medium Magnification	High Magnification
Standard time for microscope control and image acquisition	~17s	~12s	~39s
Standard time for image processing	~3s	~15s	~1s

Table 2

Table 1 Examples of automatic run experimental results

Number of grids	Number of images				Time
	Low magnification	Medium magnification	High magnification	Total	
96	1651	1351	3012	6014	50h25
58	400	569	1018	1987	21h09
96	1004	1305	3278	5587	59h17
55	592	936	1623	3151	37h43
41	454	696	1067	2217	22h23
96	1254	1751	3229	6234	59h08

Table 3

Table 1 Acquisition conditions used for the tests

Image index	Exposure time	Illumination	Magnification
1	0.2	0.4	1350*
2	0.3	0.4	1350*
3	0.4	0.4	1350*
4	0.5	0.4	1350*
5	0.6	0.4	1350*
6	0.7	0.4	1350*
7	0.7	0.6	1350*
8	0.7	0.7	1350*
9	0.7	0.8	1350*
10	0.7	0.9	1350*
11	0.7	1.0	1350*
12	0.7	0.4	560
13	0.7	0.4	890
14	0.7	0.4	1350
15	0.7	0.4	1700
16	0.7	0.4	2200
17 to 22	0.7	0.4	1350